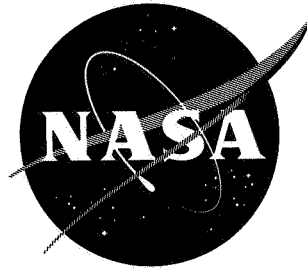NASA TN D-1016

TECHNICAL NOTE

D-1016

JET EFFECTS ON CYLINDRICAL AFTERBODIES HOUSING SONIC AND

SUPERSONIC NOZZLES WHICH EXHAUST AGAINST A

SUPERSONIC STREAM AT ANGLES OF ATTACK FROM 90° TO 180°

By Lovick O. Hayman, Jr., and Russell W. McDearmon

Langley Research Center
Langley Air Force Base, Va.

NATIONAL AERONAUTICS AND SPACE ADMINISTRATION

WASHINGTON   March 1962

NATIONAL AERONAUTICS AND SPACE ADMINISTRATION

TECHNICAL NOTE D-1016

JET EFFECTS ON CYLINDRICAL AFTERBODIES HOUSING SONIC AND

SUPERSONIC NOZZLES WHICH EXHAUST AGAINST A

SUPERSONIC STREAM AT ANGLES OF ATTACK FROM 90° TO 180°

By Lovick O. Hayman, Jr., and Russell W. McDearmon

SUMMARY

An investigation has been made to determine jet effects on cylindrical afterbodies housing sonic and supersonic nozzles which exhaust against a supersonic stream at angles of attack from 90° to 180°. The tests were conducted at a free-stream Mach number of 2.91 and at free-stream Reynolds numbers, based on body diameter, of 0.15×10^6 and 0.30×10^6. The range of the ratio of jet total pressure to free-stream static pressure investigated was from jet off to about 400.

The data presented herein showed that, in general, variation of the ratio of jet total pressure to free-stream static pressure, jet-exit Mach number, and ratio of jet-exit diameter to body diameter had large influences on the body pressures on the windward halves of the afterbodies and negligible influences on the leeward pressures. There was a negligible effect of Reynolds number on the body pressures. The ratio of jet total pressure to free-stream static pressure also had a large influence on the base pressures at all angles of attack. Schlieren studies showed details of the shock-wave structure caused by the jet and the extent of the jet interference flow fields.

INTRODUCTION

In the design of high-performance aircraft, missiles, and spacecraft, many problem areas exist in which an understanding of the complex flow phenomena associated with gas jets exhausting into a free stream at angles ranging from normal to the stream to directly against the stream would be helpful. Foremost among these problem areas is the interference of jets with adjacent surfaces. For example, bomber defense missiles may experience angles of attack from 90° to 180° immediately after launch from the bomber (see ref. 1). During this period of high angle of attack, hot exhaust gases from the rocket engine could damage the missile structurally and could induce loads on the aft end which would alter the

stability and control characteristics of the missile. Also reaction-control jets, which are currently used on high-performance aircraft such as the X-15 (see ref. 2) and in the separation of rocket stages (see ref. 3) and which undoubtedly will be used extensively on space vehicles in the future, may experience angles of attack from 90° to 180°. These jets may induce significant short-duration loads on adjacent surfaces. Some of these interference effects have been investigated in references 4 to 8.

Some possible applications of jets exhausting against a stream are as follows: (1) Jets may be used for deceleration of space vehicles in planetary atmospheres. Although the "brute force" technique of braking a reentering vehicle by use of a large retrorocket is unattractive because of the large fuel requirements of present-day chemical rockets, the probable eventual development of nuclear rockets may cause this technique to become attractive in the future. (See ref. 9.) (2) Aerodynamic heating may be alleviated by use of jets. One method of cooling a blunt body or wing is to eject a cold gas from its nose or leading edge. Some of the factors involved in cooling by this method were explored in references 10 and 11. (3) Jets may be used to alter aerodynamic drag. The drag of blunt bodies or wings may be altered by exhausting a small jet from the nose or leading edge. In references 12 and 13 this technique was investigated for some blunt bodies.

Presented herein are the results of an investigation of the effects of systematic variations of the ratio of jet total pressure to free-stream static pressure on cylindrical afterbodies housing sonic and supersonic nozzles which exhaust into a supersonic stream at angles of attack from 90° to 180°. Limited investigations were made of the effects on the afterbodies of jet-exit Mach number, the ratio of jet-exit diameter to body diameter, and Reynolds number. The purpose of these tests was to obtain basic information on the interactions of the jets, free stream, and afterbodies, which should be applicable to the problem areas mentioned previously. The free-stream Mach number was 2.91, the Reynolds numbers, based on body diameter, were 0.15×10^6 and 0.30×10^6, and the range of the ratio of jet total pressure to free-stream static pressure was from jet off to about 400. Pressure distributions on the afterbodies and the jet-exit annuli were measured, and schlieren photographs of the flow fields around the afterbodies were taken.

SYMBOLS

$\dfrac{A_e}{A^*}$ ratio of area of maximum jet-flow expansion in external stream to area of nozzle throat

C_p pressure coefficient, $\dfrac{p - p_\infty}{q_\infty}$

D twice the distance along axis of symmetry from afterbody base to interface between jet and free stream (see fig. 19)

d afterbody diameter

d_e diameter of maximum jet-flow expansion in the external stream

d' diameter of plane segment bounded by locus of points obtained by intersection of interface surface with cone determined by angle for shock detachment (see fig. 18)

F distance along body axis of symmetry measured from the afterbody base to a point on the bow shock

M Mach number

p static pressure

p_t stagnation pressure

$\dfrac{p_{t,j}}{p_\infty}$ jet pressure ratio

q dynamic pressure

R Reynolds number

r_b radius of base

r_o radial distance to pressure orifice

x distance from body base measured along body axis of symmetry

x_i distance from body base to "induced" shock, measured parallel to body axis of symmetry (see fig. 10(a))

x' distance along body axis of symmetry from most forward point on bow shock to plane containing d' (see fig. 18)

y distance normal to body axis of symmetry

α angle of attack

δ_{det} angle for shock detachment (see fig. 18)

ϕ angle between a meridian plane containing orifices and reference meridian plane which is perpendicular to angle-of-attack plane (see fig. 2)

Subscripts:

b   base

j   jet

max   maximum

min   minimum

∞ free stream

1   conditions just upstream of a normal shock

2   conditions just downstream of a normal shock

APPARATUS

Wind Tunnel

All tests were conducted in the Langley 9-inch supersonic tunnel (recently deactivated), which was a continuous-operation, closed-circuit type of tunnel in which the pressure, temperature, and humidity could be controlled. The test section was approximately square. A low turbulence level in the test section was attained by the installation of 11 fine-mesh turbulence-damping screens in the settling chamber ahead of the supersonic nozzle. A schlieren optical system was provided for qualitative flow observations. Throughout the tests the dewpoint of the tunnel flow was kept low enough to insure that the effects of condensation were negligible.

Models, Support, Instrumentation, and Air Supply for Jets

Figure 1 presents drawings of the three models used in the present investigation. The models were cylinders which were identical externally. Model 1 housed a sonic nozzle, and models 2 and 3 housed supersonic

nozzles having exit Mach numbers of 3. Models 1 and 2 had an exit or base annulus, and model 3 had a sharp lip at the nozzle exit.

A line of orifices was installed in the external cylindrical sur- face of each model. These orifices extended from near the exit to approximately 4 body diameters ahead of the exit. The spacing of these orifices is given in the table of figure 1. Model 1 had two orifices on the exit annulus, each having a different radial location, and model 2 had only one orifice on the annulus. Pressure measurements were obtained in three meridian planes around the cylinders and annuli by rolling the models between each test (see fig. 2). The pressures were measured by a multitube mercury manometer.

The models were supported in the tunnel by bent stings. These stings were bent at angles of 30°, 60°, and 90° in order to obtain the angle-of-attack range of the investigation (90° to 180°). Dry air from high-pressure storage tanks was conveyed to the model plenum chambers by a flexible hose which was attached to the downstream ends of the stings. The jet stagnation pressures were measured by a Bourdon gage in a 2-inch-diameter pipe to which the flexible hose was connected immediately outside the tunnel.

TESTS AND ACCURACY

The tests were conducted at a free-stream Mach number of 2.91, and at Reynolds numbers, based on model diameter, of 0.15×10^6 and 0.30×10^6. Pressure distributions over the external cylindrical surfaces of each model and over the exit annuli of models 1 and 2 were measured, and schlieren photographs of the flow fields around the models were taken at angles of attack of 90°, 120°, 150°, 170°, and 180°. At each angle of attack, schlieren photographs and pressure measurements were taken for the jet-off condition and for jet pressure ratios from approximately 30 to 400. The pressure-measurement coverage consisted of measurements on the windward and leeward sides of the models in the angle-of-attack plane and in planes 45° and 90° from the angle-of-attack plane.

The estimated probable errors in the test parameters and variables were as follows:

$\dfrac{p_{t,j}}{p_\infty}$, percent . . . . ±2.0

M . . . . ±0.01

C_p . . . . ±0.01

α, deg . . . . ±0.10

The angle of yaw of the models was maintained at 0°, within ±0.10°.

6

RESULTS AND DISCUSSION

Flow Phenomena in the Vicinity of the Afterbody Base

Figure 3 presents a schlieren photograph and a simplified sketch of the flow phenomena in the vicinity of the base of model 1 at $\alpha = 180^\circ$. Some insight into the mechanism of the interaction of the free-stream flow and jet flow may be gained from this figure. The wave system consisted of a bow shock, a jet shock which terminated at the jet boundary, a secondary shock, and two expansion fans. An interface also appeared which was a boundary between the jet and free-stream flows. At any point along the interface, flows adjacent to it had equal pressures; however, the interface was not a boundary of constant pressure. Typical free-stream and jet streamlines are also shown in figure 3. The streamlines coinciding with the axis of symmetry had a mutual stagnation point. The flow field will be further analyzed in a subsequent section.

General effects of jet pressure ratio.- Figures 4, 5, and 6 present schlieren photographs of the flow phenomena in the vicinity of the bases of models 1, 2, and 3, respectively, for angles of attack from 90° to 180°. The Reynolds number was 0.15×10^6.

At $\alpha = 90^\circ$, the jet flow was remote from the afterbodies as it turned downstream. At $\alpha = 120^\circ$, it appears that the jet flow remained clear of the afterbodies; however, at the higher jet pressure ratios some jet spillage may have occurred on the windward half of the afterbodies. Increasing the angle of attack from 120° to 150° caused a large increase in the amount of afterbody that was encompassed by the jet flow. Further increase of angle of attack to 180° affected the amount encompassed only slightly. As would normally be expected, the jet flow was ejected progressively farther from the base and had a larger area of maximum jet-flow expansion as the jet pressure ratio was increased at all angles of attack.

Effect of jet-exit Mach number.- Comparisons of the flow fields of model 1, model 2, and model 3 (figs. 4, 5, and 6) indicate the following effects of jet-exit Mach number on the flow phenomena in the vicinity of the model base: (1) At $\alpha = 170^\circ$ and 180°, the jet flow was ejected farther from the base for the models with the supersonic jet than for the model with the sonic jet. (2) At all angles of attack, the jet flow from the models with the supersonic jet had a smaller angle of inclination of the jet boundary at the exit than the model with the sonic jet. (3) Considerable mixing between the free-stream and jet flow was indicated in the vicinity of the base for the supersonic jet whereas the sonic jet had a clearly defined interface or boundary between the flows.

Body Pressures

General effects of jet pressure ratio.- Figures 7, 8, and 9 present
the effects of jet pressure ratio on the pressure distributions in three
meridian planes for models 1, 2, and 3, respectively, for angles of
attack from 90° to 180°. The Reynolds number was 0.15×10^6.

The windward pressures were influenced considerably by jet pressure
ratio. In general, an increase in jet pressure ratio brought about a
decrease in pressure coefficient at any given point on the body. The
greatest changes in the windward pressures on a major portion of the
afterbody due to variation in jet pressure ratio occurred for angles of
attack from 120° to 170°. The leeward pressures changed very little
with jet pressure ratio and were near free-stream pressure for all angles
of attack.

Effect of jet-exit Mach number and ratio of jet-exit diameter to
body diameter.- Comparisons of the results for models 1, 2, and 3 indi-
cate that the effects on the pressure distributions due to exit Mach
number (figs. 7 and 8) and ratio of jet-exit diameter to body diameter
(figs. 8 and 9) generally occurred for angles of attack less than 170°
and on the windward half of the afterbodies. The largest effects occur-
red at $\alpha = 120^\circ$ and 150°. In general, the leeward pressures were not
influenced by jet-exit Mach number and ratio of jet-exit diameter to
body diameter.

Comparison of figures 7 and 8 at $\alpha = 120^\circ$ shows that peaks in
the pressure distributions on the windward half of the body occurred
for the sonic model but did not occur for the model with a supersonic
Mach number. The schlieren photographs of the sonic jet at this angle
of attack in figure 4(b) show a disturbance approximately normal to the
windward side of the afterbody. When shocks of the same family (in this
case the bow and secondary shocks) intersect, a weak compression or
expansion wave usually emanates from the point of intersection. Results
obtained with the use of oblique-shock relations and measured shock
angles indicate the wave to be a weak shock which will be referred to
hereafter as the "induced" shock. A simplified sketch of the flow field
showing this induced shock is presented in figure 10(a) for an angle of
attack of 120°. Figure 10(b) presents the location of the induced shock
as a function of jet pressure ratio and also indicates the ratio at
which the shock appeared initially. (The locations were scaled from
the schlieren photographs.) The induced-shock locations of figure 10(b)
correlate with the peak-pressure locations of figure 7.

Figure 5(b) shows that at the same angle of attack ($\alpha = 120^\circ$), for
the supersonic model (model 2) the bow shock and secondary shock did not
intersect; hence, the induced shock did not occur. Increasing the ratio
of jet-exit diameter to body diameter from 0.8 (model 2) to 1.0 (model 3)

with the supersonic jet caused small peaks to occur in the pressure dis-
tributions for $x/d > 1/2$ (compare figs. 8(a) and 9(a)). However, it
is difficult to discern from the schlieren photographs of model 3 in
figure 6(b) whether these peaks are related to an induced shock. A
cusp in the bow shock (similar to cusp seen in fig. 4(b)) did occur
near the base of the model, but a secondary shock and induced shock are
not clearly evident.

Comparison of figures 7 and 8 at $\alpha = 150^\circ$ shows that the decrease
in level of the pressure distributions near the model base on the wind-
ward side for a given increase in jet pressure ratio was greater for the
model with the sonic jet (model 1) than for the model with the supersonic
jet (model 2). Comparison of figures 8 and 9 at $\alpha = 150^\circ$ shows that
increasing the ratio of jet-exit diameter to body diameter from 0.8
(model 2) to 1.0 (model 3) with the supersonic jet reduced the level of
the pressure distributions near the base but not to the level of the model
with the sonic jet (fig. 7). It should be noted that there is a small
difference in the nozzle half angles of models 2 and 3.

Effect of Reynolds number.- Figures 11, 12, and 13 show that for
the Reynolds number range of these tests, Reynolds number had a neg-
ligible effect on the pressure distributions of models 1, 2, and 3,
respectively.

Base Pressures

Figures 14, 15, and 16 present the effects of jet pressure ratio on
the base pressures of models 1 and 2. The base pressures were measured
at two radial locations for model 1 and one radial location for model 2.
The Reynolds number was 0.30×10^6.

In discussing the base pressures, the half of the base annulus
corresponding to the windward half of the body will be referred to as
the "windward half of the annulus," and the half corresponding to the
leeward half of the body as the "leeward half of the annulus."

Figure 14 shows that on the windward half of the annulus of model 1
at $\alpha = 90^\circ$, the pressures increased from below free-stream static pres-
sure at jet-off to near normal-shock recovery pressure ($C_{p,b} = 1.75$) at
the highest jet pressure ratio. This effect was consistent with the
fact that the angle of inclination of the bow shock near the base became
more nearly normal to the free-stream direction as jet pressure ratio
was increased. (See the schlieren photographs of fig. 4(a).) The pres-
sures on the leeward half of the annulus were near free-stream pressure
at jet off and decreased slightly as jet pressure ratio was increased.

When the angle of attack was increased to 120°, the base pressures on the windward half of the annulus reached a peak near $\frac{P_{t,j}}{P_\infty} = 80$ and then decreased to below jet-off values as jet pressure ratio was increased.

At angles of attack from 170° to 180°, the annulus pressures of model 1 decreased from near normal-shock static pressures ($C_{p,b} = 1.47$) at jet-off to below free-stream static pressure as jet pressure ratio was increased. The pressures usually became symmetric over the annulus for a jet pressure ratio of 27 and showed only slight change as the jet pressure ratio was further increased.

Comparison of figures 14 (orifice location at $r_o/r_b = 0.582$) and 15 ($r_o/r_b = 0.848$) shows that, in general, the same trends in effects of jet pressure ratio on the base pressures of model 1 occurred for both orifice locations, except at $\alpha = 90°$ and 120°. At these angles of attack, the pressures measured by the outer orifice were, in general, lower than those measured by the inner orifice.

Figure 16 shows that the pressures on the windward half of the annulus of model 2 at $\alpha = 150°$ increased to a peak near $\frac{P_{t,j}}{P_\infty} = 45$ and then decreased below jet-off values as jet pressure ratio was increased further. These results were considerably different from those obtained for model 1, and these differences might be explained by a comparison of figures 4(c) and 5(c), which reveals that the secondary shock remained near the base of model 2 to higher values of jet pressure ratio than for model 1.

Comparisons of figures 14(d) and 14(e) with 16(b) and 16(c) show that at $\alpha = 170°$ and 180°, generally the same trends in the pressure distributions on the annuli were obtained for models 1 and 2, except that a higher jet pressure ratio was required to obtain symmetric pressures over the base of model 2.

Prediction of the Shock Structure in the Vicinity of the Base of Model 1 at $\alpha = 180°$

The analysis to be described in this section was only applied to model 1 at an angle of attack of 180° since the prediction of the flow field depends on the use of experimental data to define the interface location. The interface was not readily visible in the schlieren

photographs of the supersonic jets, and at angles of attack other than 180° the interface for model 1 had a complex, nonsymmetrical shape. Thus a semiempirical prediction of the flow was not attempted at these conditions. Figure 17 presents the experimental variation of interface detachment distance parameter D/d with jet pressure ratio for model 1 at $\alpha = 180°$. The smooth variation in interface location with jet pressure ratio enabled the data points to be fitted by a simple equation which is given in figure 17.

In the schlieren photographs of model 1 at $\alpha = 180°$ (fig. 4(e)), the bow shocks are seen to resemble those in front of blunt bodies. Assuming that the jet flow within the interface can be represented by a solid body with a hemispherical nose enables the bow-shock location and shape to be predicted by using the method presented in reference 14. The shape of the interface was found to approximate closely the surface of a hemisphere with center at the model base and radius $D/2$ the distance along the axis of symmetry from the model base to the interface. Figures 18 and 19 present the experimental (scaled from schlieren photos) and theoretical variations of bow-shock detachment distance and shape with jet pressure ratio. The close agreement between experiment and theory indicates that the jet flow within the interface may be treated as a solid body. The experimental bow-shock detachment distances and shapes (fig. 19) were seen to be unaffected by both Reynolds number and jet pressure ratio when the shock coordinates were nondimensionalized by the distance D. Included in figure 19 are the nondimensionalized coordinates of the afterbody for each experimental combination of Reynolds number and jet pressure ratio. The bow-shock location and shape can be readily determined at any desired jet pressure ratio within the range of experimental data by using the equation given in figure 17 and the curves of figures 18 and 19. It should be noted that even though the shape of the interface will be affected to some extent by the ratio of jet-exit diameter to body diameter, these results should still be applicable for many other configurations since there is only a small effect of nose shape upon bow-shock location and shape upstream of the sonic point unless the nose tip is in close proximity to the detached shock.

Prediction of the maximum expansion of the jet flow may be made from knowledge of the free-stream properties and use of one-dimensional channel theory and normal-shock theory, since a mutual stagnation point exists. For a given jet pressure ratio, the jet total pressure ratio at a given free-stream Mach number can be determined from the following simple equation:

$$\frac{p_{t,j2}}{p_{t,j1}} = \frac{p_\infty}{p_{t,j1}} \frac{p_{t,1}}{p_\infty} \frac{p_{t,2}}{p_{t,1}}$$

where $p_{t,2} = p_{t,j2}$. The area ratio of the maximum expansion corresponding to a given jet total pressure ratio may be determined from compressible-flow tables. (See, for example, ref. 15.) Figure 20 presents the experimental variation of the maximum jet-flow expansion with jet pressure ratio and the prediction of one-dimensional channel theory and normal-shock theory. The spread in experimental data for a given jet pressure ratio was a consequence of the finite width of the jet boundary as it appeared on the schlieren photographs (see fig. 4(e) and sketch in fig. 20) in the region of the maximum expansion. An average of the extreme area ratios as they appeared on the photographs was in fair agreement with the one-dimensional prediction. The experimental area ratios indicate that there was no effect of Reynolds number.

SUMMARY OF RESULTS

The results of an investigation to determine jet effects on cylindrical afterbodies housing sonic and supersonic nozzles which exhaust against a supersonic stream at angles of attack from 90° to 180° indicate the following:

1. The jet flow was remote from the afterbodies as it turned downstream at an angle of attack of 90°. At an angle of attack of 120°, most of the jet flow seemed to remain remote; however, at the higher jet pressure ratios some jet spillage might have occurred on the windward half of the afterbodies. Increasing the angle of attack from 120° to 150° caused a large increase in the amount of afterbody that was encompassed by the jet flow. Further increase of angle of attack to 180° affected the amount encompassed only slightly.

2. Large effects of jet pressure ratio on body pressure distributions were obtained at angles of attack from 120° to 170° on the windward halves of the afterbodies. In general, small effects were obtained on the leeward halves at all angles of attack.

3. Schlieren photographs showed a clearly visible interface between the jet flow and the free-stream flow for the model with the sonic jet. At an angle of attack of 180°, this interface was nearly hemispherical in shape. For the models with a supersonic jet the interface was usually not visible since a mixing between the jet flow and the free-stream flow occurred.

4. The largest effects of jet-exit Mach number and ratio of jet-exit diameter to body diameter on the body pressure distributions occurred at angles of attack of 120° and 150° on the windward halves of the afterbodies. In general, the leeward pressures were not influenced by exit Mach number and ratio of jet-exit diameter to body diameter.

5. The jet flow produced large effects on the base pressures at all angles of attack. The magnitudes of the base pressures ranged from approximately normal-shock recovery pressure to below free-stream static pressure.

6. Increasing the Reynolds number, based on body diameter, from 0.15×10^6 to 0.30×10^6 had negligible effects on the body pressures.

7. The case of the sonic jet exhausting directly upstream ($\alpha = 180^\circ$) lent itself to a simple semiempirical prediction of the shock structure, and fair agreement was obtained between this prediction and experiment.

Langley Research Center,
    National Aeronautics and Space Administration,
        Langley Air Force Base, Va., November 7, 1961.

REFERENCES

1. Anon.: Jet-Vane Controlled Bomber Defense Missile. Rep. No. BE-753-S4 (Contract AF 33(038)-22346), Cornell Aero. Lab., Inc., July-Sept. 1951.

2. Boskovich, Boris, Cole, George H., and Mellen, David L.: Advanced Flight Vehicle Self-Adaptive Flight Control System. Part I - Study. WADD Tech. Rep. 60-651, U.S. Air Force, Sept. 30, 1960.

3. Horsewood, J. L.: Methods to Alter Flight Path of Delta Third Stage After Burnout Model DM 19. Rep. No. SM-36395 (Contract NASw-38), Douglas Aircraft Co., Inc., Feb. 18, 1960.

4. Romeo, David J., and Sterrett, James R.: Aerodynamic Interaction Effects Ahead of a Sonic Jet Exhausting Perpendicularly From a Flat Plate Into a Mach Number 6 Free Stream. NASA TN D-743, 1961.

5. Cubbison, Robert W., Anderson, Bernhard H., and Ward, James J.: Surface Pressure Distributions With a Sonic Jet Normal to Adjacent Flat Surfaces at Mach 2.92 to 6.4. NASA TN D-580, 1961.

6. Janos, Joseph J.: Loads Induced on a Flat-Plate Wing by an Air Jet Exhausting Perpendicularly Through the Wing and Normal to a Free-Stream Flow of Mach Number 2.0. NASA TN D-649, 1961.

7. Bressette, Walter E., and Leiss, Abraham: Effects on Adjacent Surfaces From the Firing of Rocket Jets. NACA RM L57D19a, 1957.

8. Vinson, P. W., Amick, J. L., and Liepman, H. P.: Interaction Effects Produced by Jet Exhausting Laterally Near Base of Ogive-Cylinder Model in Supersonic Main Stream. NASA MEMO 12-5-58W, 1959.

9. Plascott, R. H.: The Re-Entry of Manned Earth Satellites. Tech. Note No. Aero 2640, British R.A.E., Aug. 1959.

10. McMahon, Howard M.: An Experimental Study of the Effect of Mass Injection at the Stagnation Point of a Blunt Body. Memo. No. 42 (Contract No. DA-04-495-Ord-19), Hypersonic Res. Project, GALCIT, May 1, 1958.

11. Watts, G. A.: An Experimental Investigation of a Sonic Jet Directed Upstream Against a Uniform Supersonic Flow. Tech. Note No. 7, Inst. Aerophys., Univ. of Toronto, Jan. 1956.

12. Love, Eugene S.: The Effects of a Small Jet of Air Exhausting From the Nose of a Body of Revolution in Supersonic Flow. NACA RM L52I19a, 1952.

14

13. Lopatoff, Mitchell: Wing-Flow Study of Pressure-Drag Reduction at Transonic Speed by Projecting a Jet of Air From the Nose of a Prolate Spheroid of Fineness Ratio 6. NACA RM L51E09, 1951.

14. Love, Eugene S.: A Reexamination of the Use of Simple Concepts for Predicting the Shape and Location of Detached Shock Waves. NACA TN 4170, 1957.

15. Ames Research Staff: Equations, Tables, and Charts for Compressible Flow. NACA Rep. 1135, 1953. (Supersedes NACA TN 1428.)

Model 1 — Exit Mach No. 1: 3.850, .050, .750, .375, .500, .030, .100, Base pressure orifices

Model 2 — Exit Mach No. 3: .050, .600, .750, .292, .500, .030, 10.90°, Base pressure orifice

Model 3 — Exit Mach No. 3: .250, .750, .365, .500, 13.52°
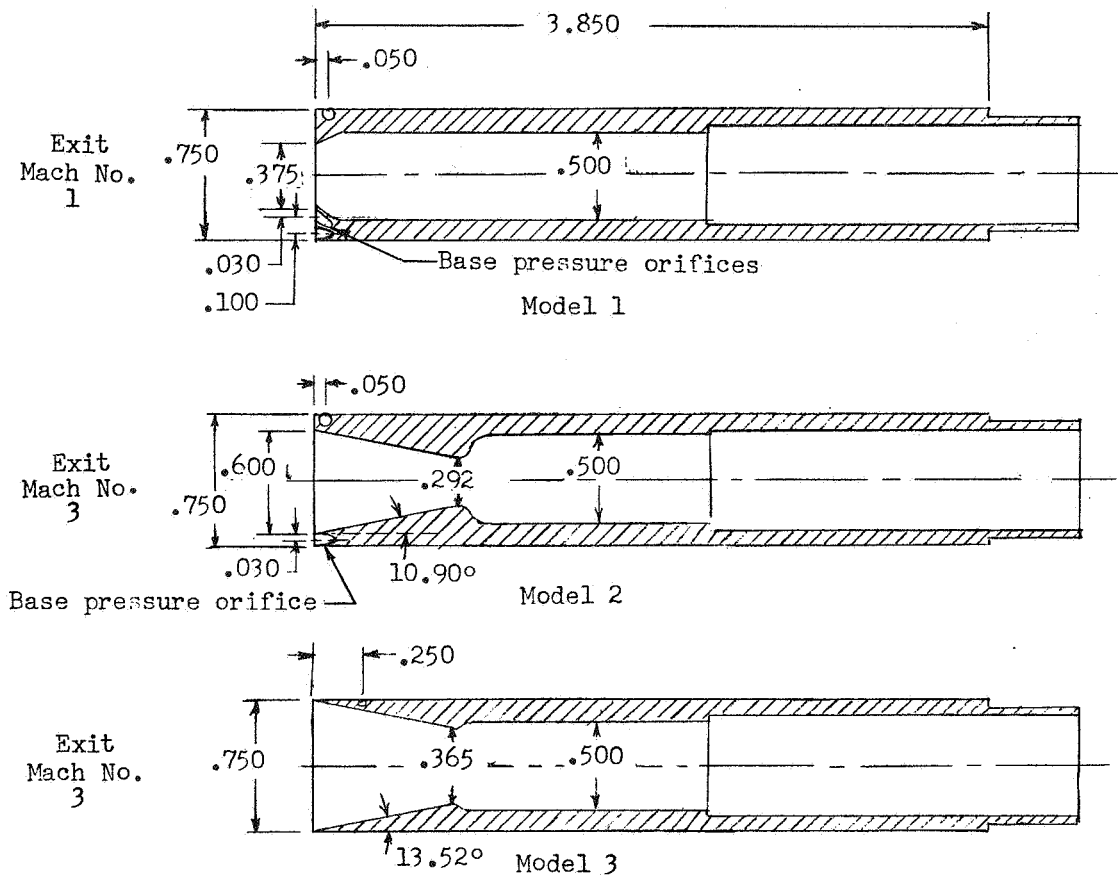
Model	Location of pressure orifices[a] on —				
	Body			Base	
	First orifice, in. ahead of base	0.100-in. spacing	0.200-in. spacing	r_o, in.	r_o/r_b
1	0.050	Next 6 orifices	Next 12 orifices	0.218 .318	0.582 .848
2	0.050	Next 6 orifices	Next 12 orifices	0.330	0.880
3	0.250	Next 10 orifices	Next 9 orifices		

[a]All orifices are in row except base orifices.

Figure 1.- Section view of models. All dimensions are in inches.
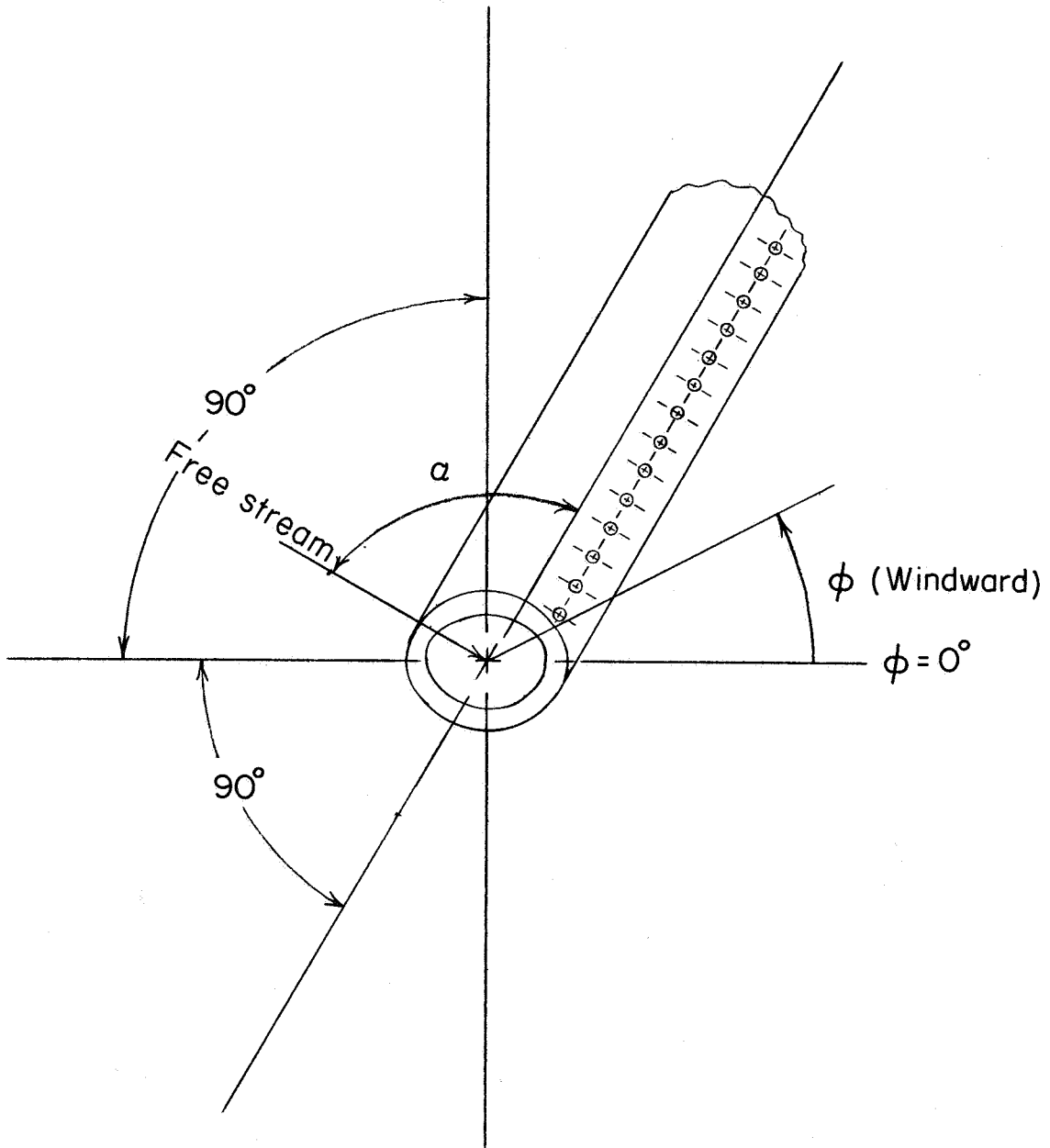
Figure 2.- Model orientation.

$M_\infty = 2.91$

Reflection of bow
shock on schlieren
window

$M_m > 1$

Bow shock

Interface

$M_\infty < 1$

$M_j < 1$

Secondary shock

Typical jet
streamline

Mutual stagnation
point

$M_j > 1$

$M_j > 1$

Jet shock

Typical streamline

Jet expansion fan

Mixing across
interface

Jet boundary

Free-stream expansion fan
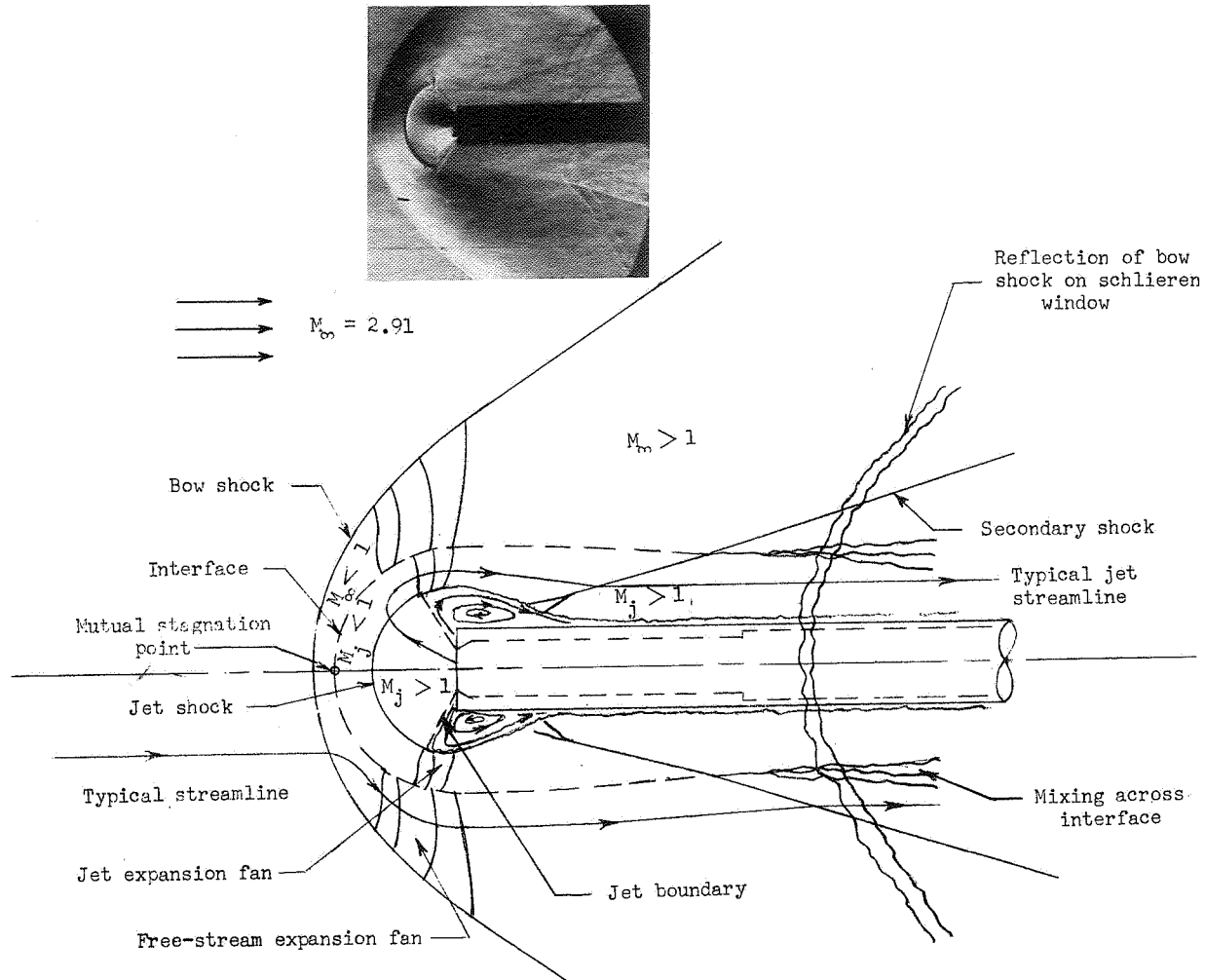
L-61-7738

Figure 3.- Schlieren and sketch of the flow phenomena in the vicinity of the base of model 1 at
$\alpha = 180^\circ$.

18
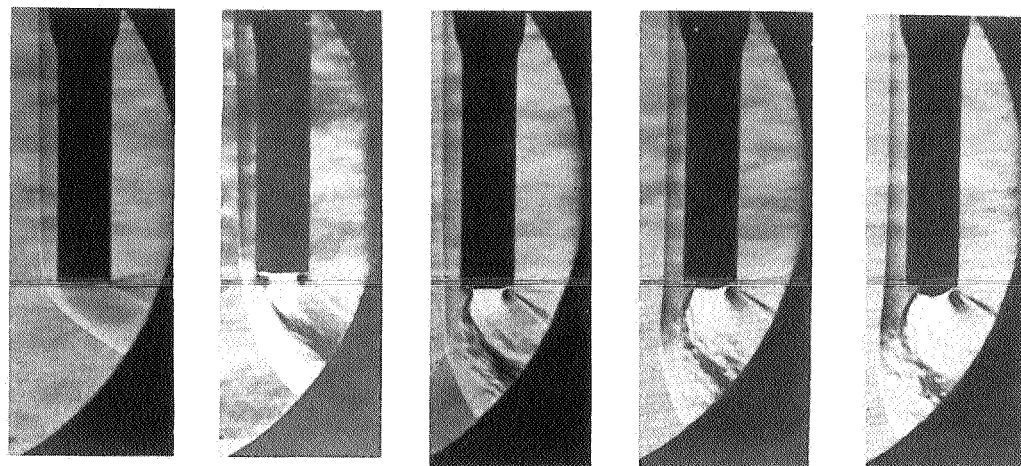
Jet off $p_{t,j}/p_\infty = 58$ 114   171   225

(a) $\alpha = 90°$.
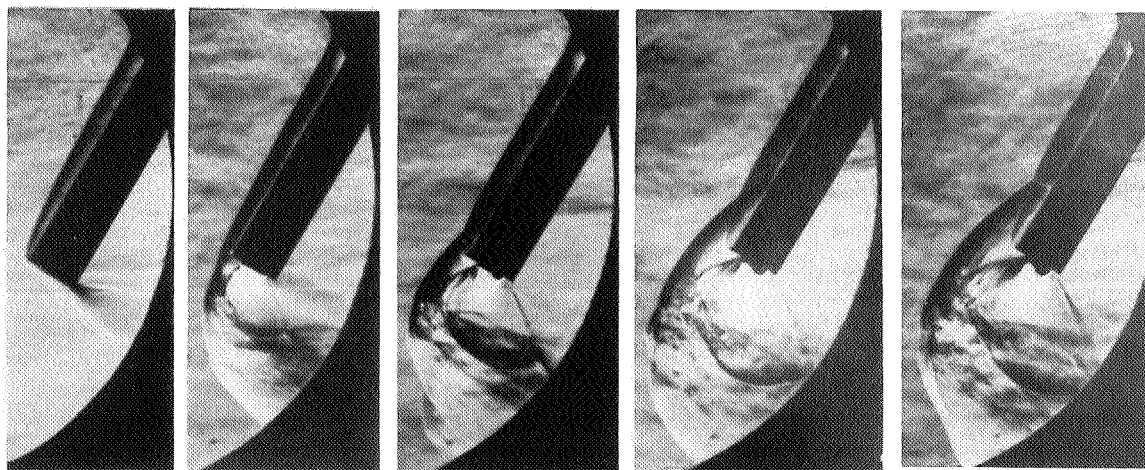
Jet off $p_{t,j}/p_\infty = 59$ 115   173   200

(b) $\alpha = 120°$.   L-61-7739

Figure 4.- Schlieren photographs of flow phenomena near base of model 1.
$R = 0.15 \times 10^6$.
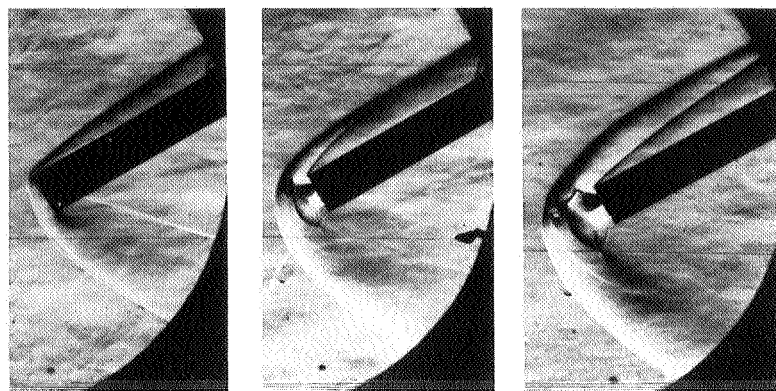
Jet off $p_{t,j}/p_\infty = 31$ 58
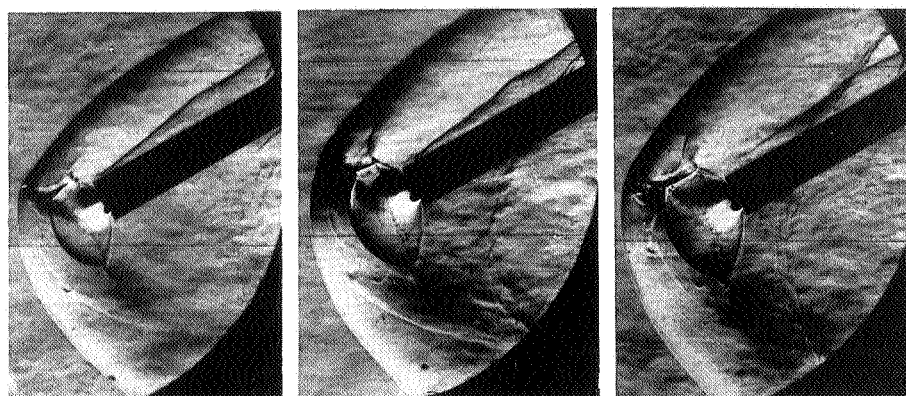
$p_{t,j}/p_\infty = 116$ 173   200
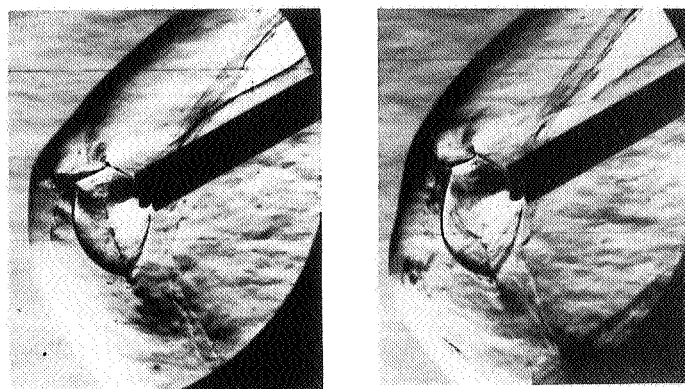
$p_{t,j}/p_\infty = 224$ 252

(c) $\alpha = 150^\circ$.   L-61-7740

Figure 4.- Continued.
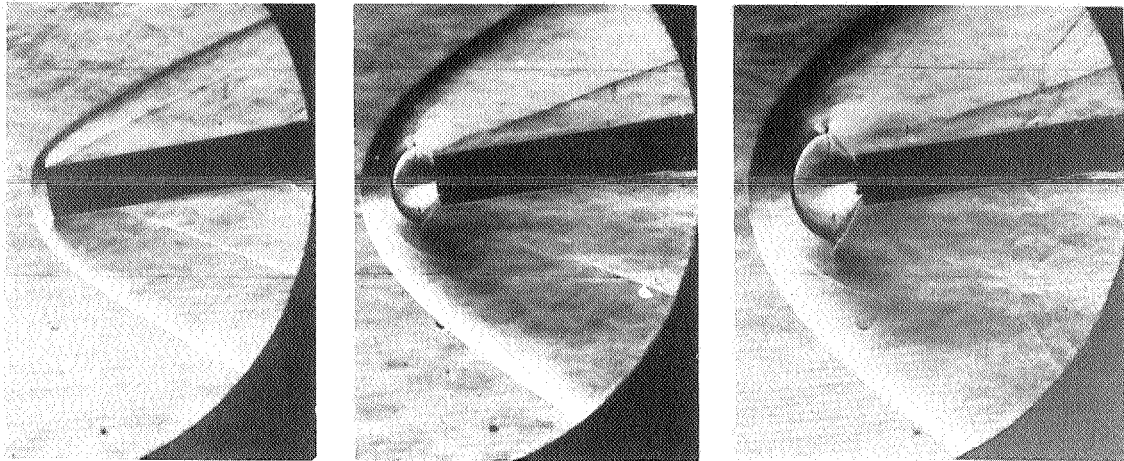
Jet off $p_{t,j}/p_\infty = 60$ 115
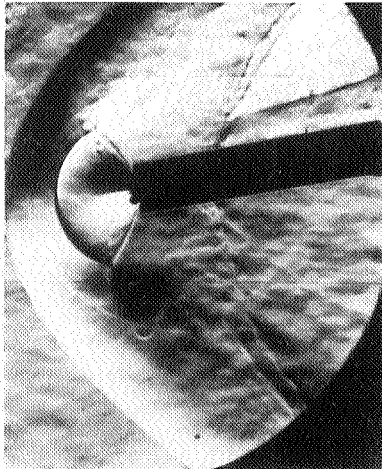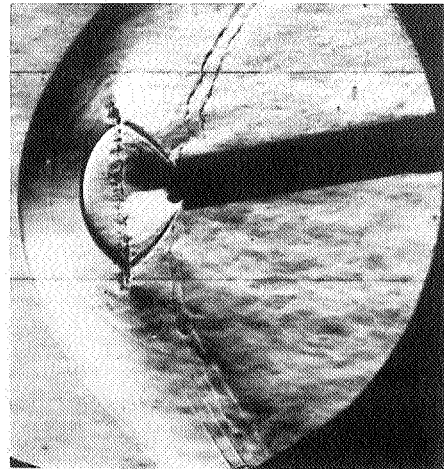
$p_{t,j}/p_\infty = 171$ 252

(d) $\alpha = 170^{\circ}$.   L-61-7741

Figure 4.- Continued.

L-1604
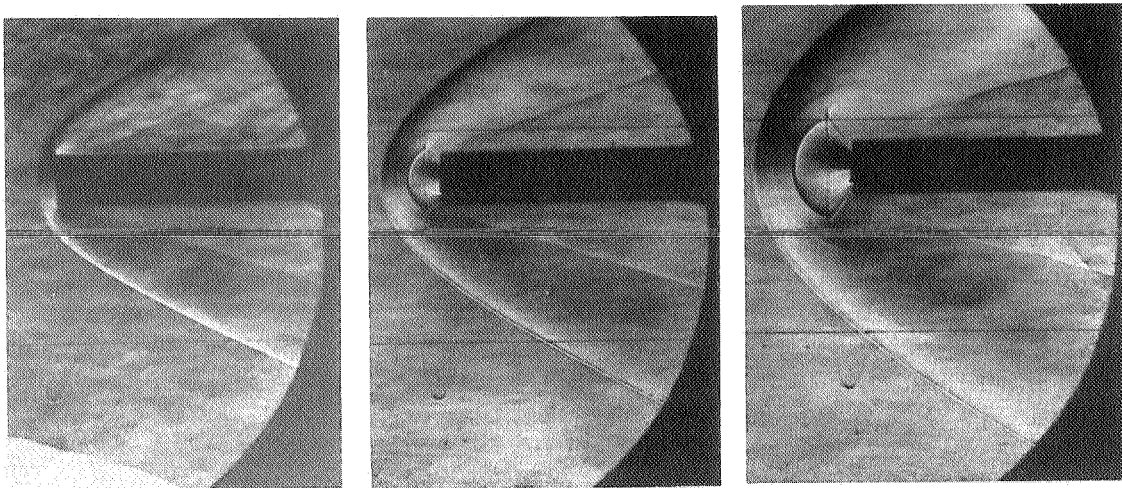
Jet off

$p_{t,j}/p_\infty = 31$

85
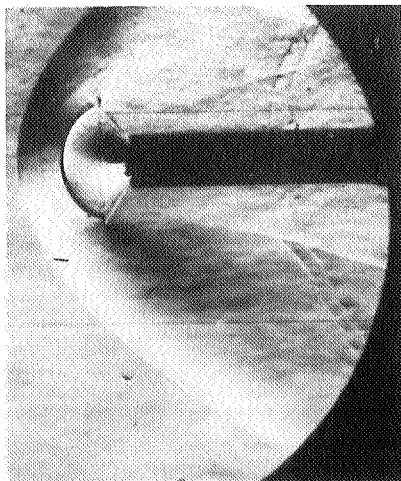
$p_{t,j}/p_\infty = 117$
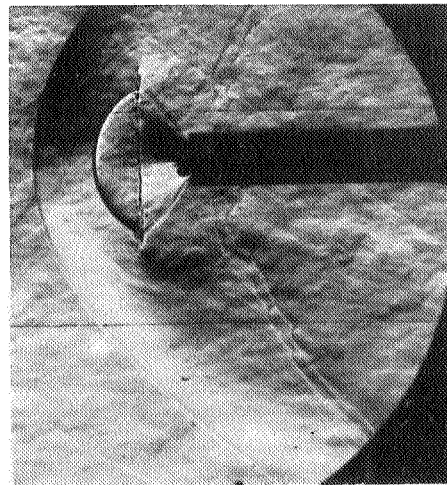
214

(e) $\alpha = 180^\circ$.

L-61-7742

Figure 4.- Concluded.
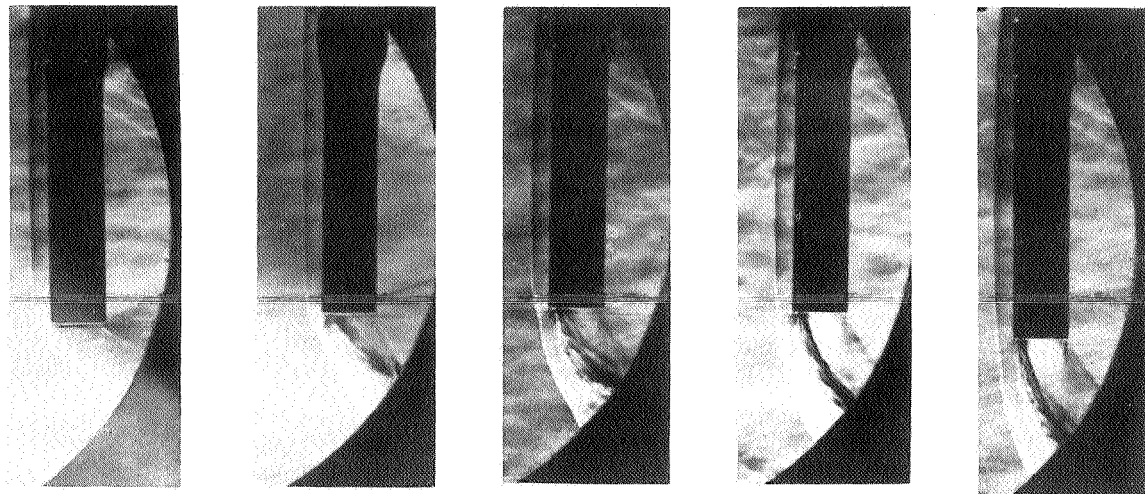
Jet off $p_{t,j}/p_\infty = 59$ 115 172 226

(a) $\alpha = 90°$.
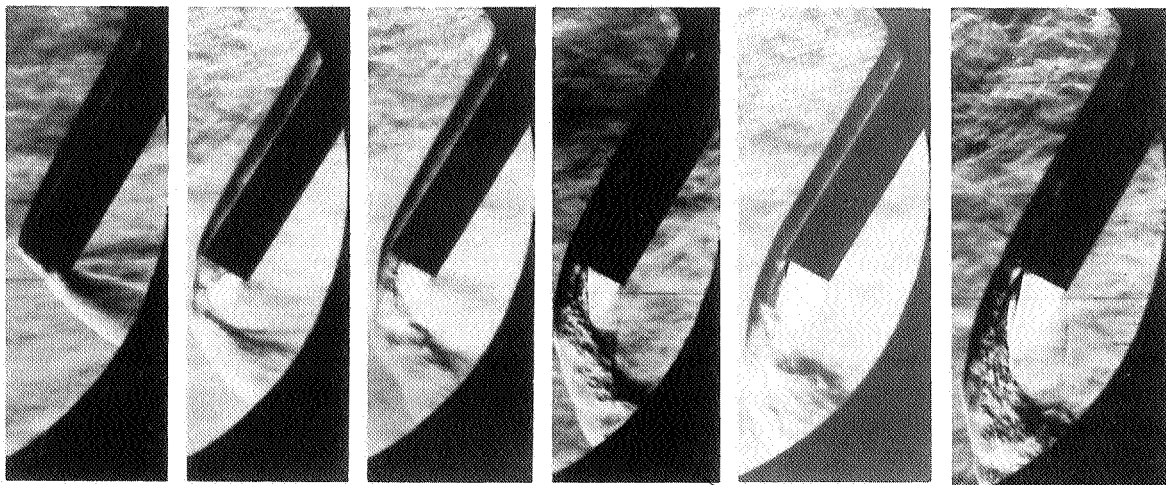
Jet off $p_{t,j}/p_\infty = 58$ 87 114 170 234

(b) $\alpha = 120°$.   L-61-7743

Figure 5.- Schlieren photographs of flow phenomena near base of model 2.
$R = 0.15 \times 10^6$.
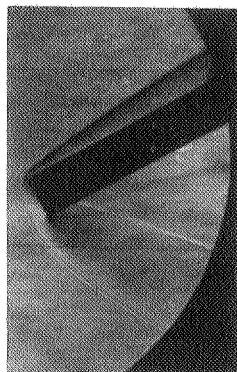
Jet off $p_{t,j}/p_\infty = 58$ 115
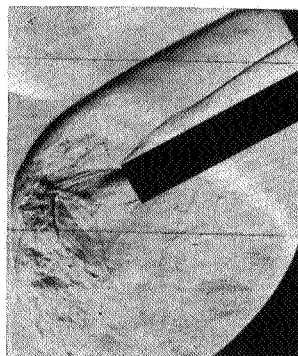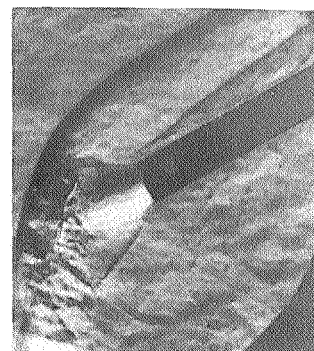
$p_{t,j}/p_\infty = 172$ 225 283
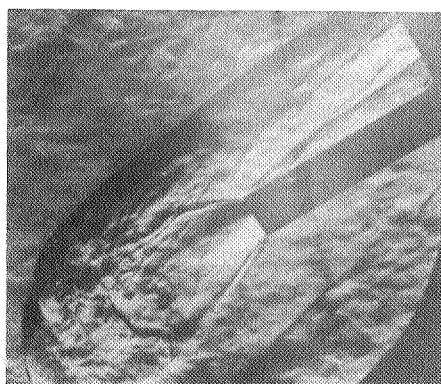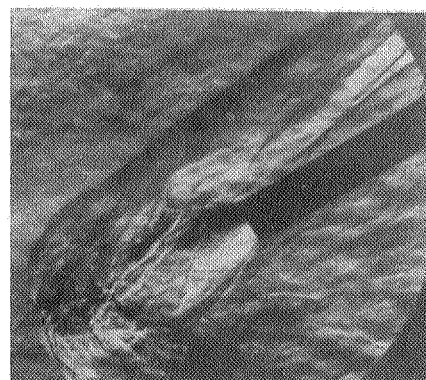
$p_{t,j}/p_\infty = 367$ 398

(c) $\alpha = 150^\circ$. L-61-7744

Figure 5.- Continued.
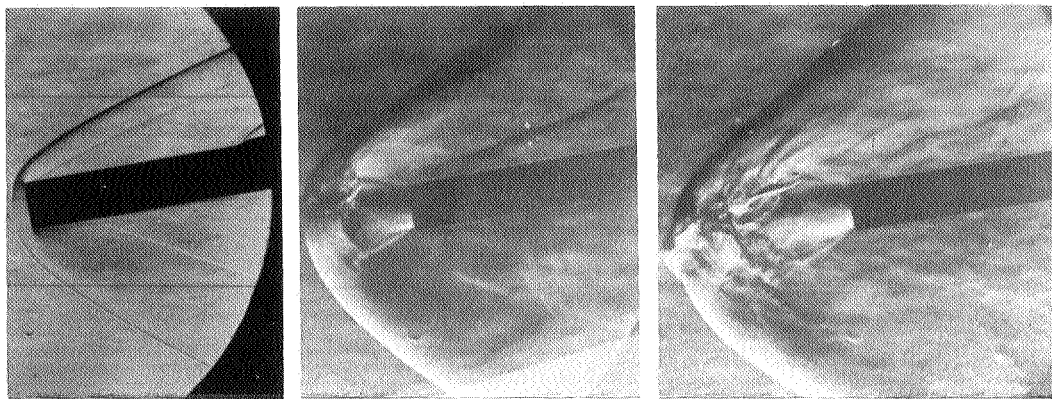
Jet off $p_{t,j}/p_\infty = 63$ 158
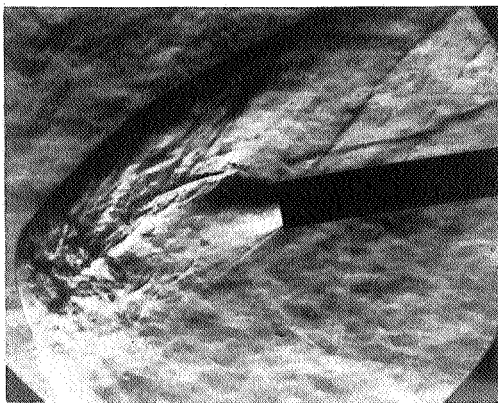
$p_{t,j}/p_\infty = 220$ 286
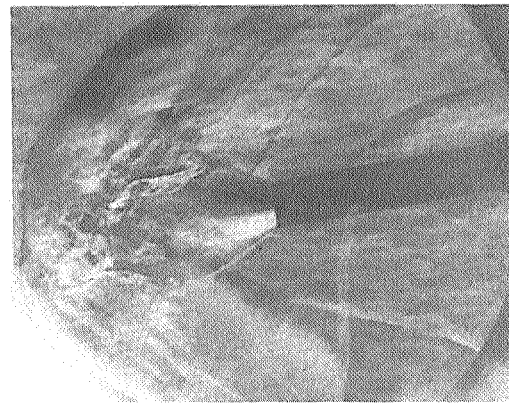
$p_{t,j}/p_\infty = 348$ 410
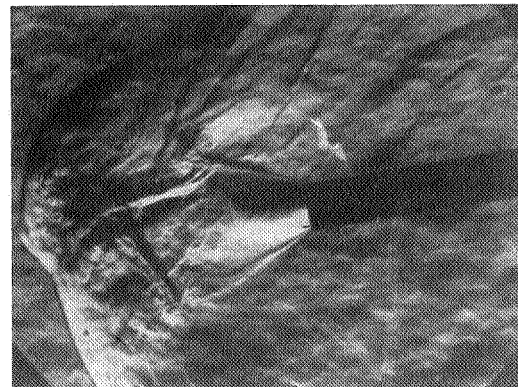
(d) $\alpha = 170^\circ$.   L-61-7745

Figure 5.- Continued.

L-1604
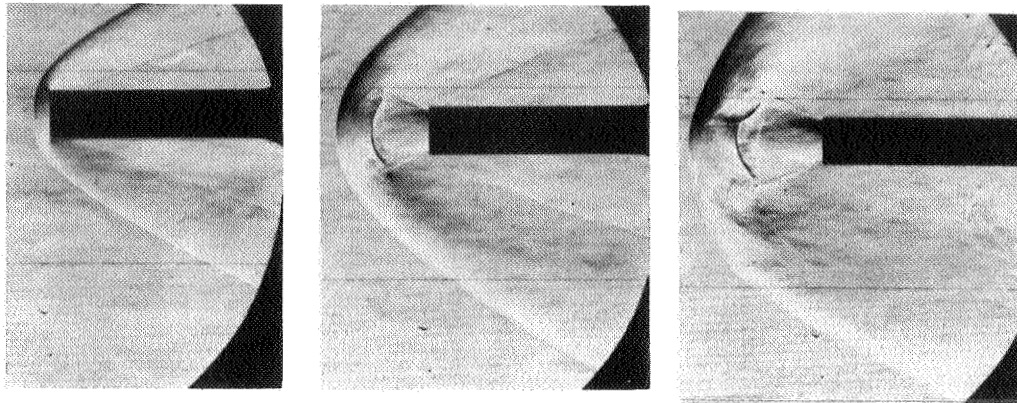
Jet off $p_{t,j}/p_\infty = 84$ 137
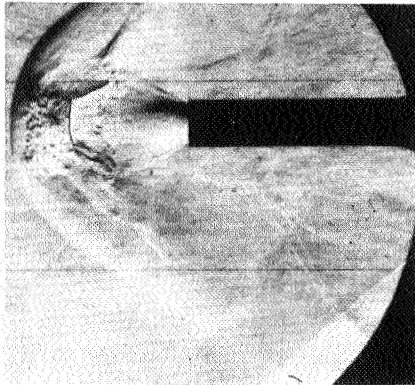
$p_{t,j}/p_\infty = 189$ 241
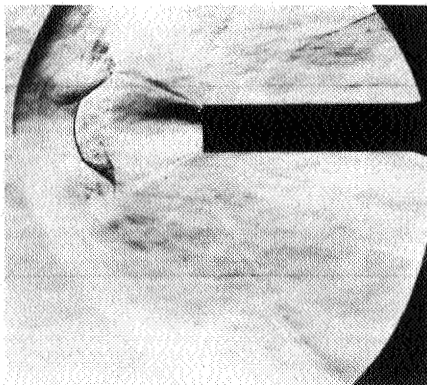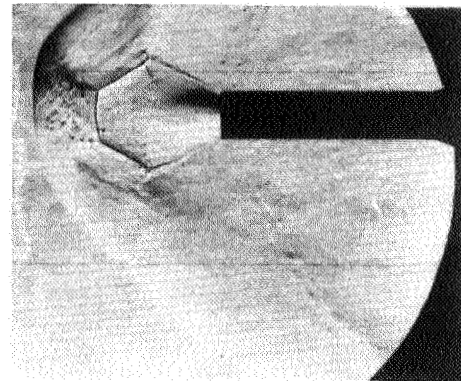
$p_{t,j}/p_\infty = 261$ 343
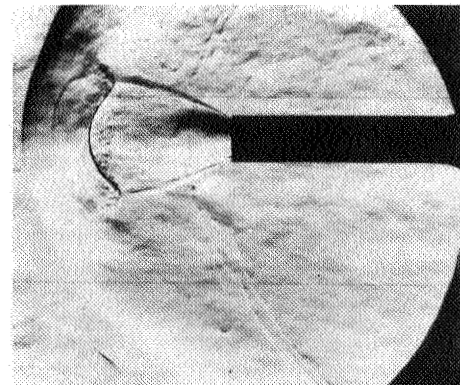
(e) $\alpha = 180^\circ$.   L-61-7746

Figure 5.- Concluded.

Jet off $p_{t,j}/p_\infty = 58$ 115   171   225

(a) $\alpha = 90°$.

Jet off $p_{t,j}/p_\infty = 58$ 115   170   223
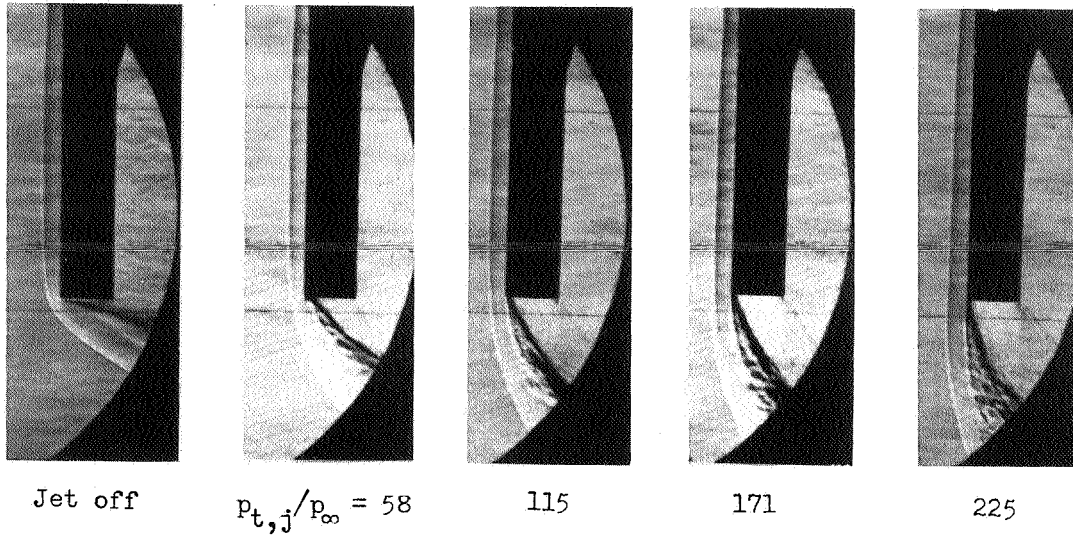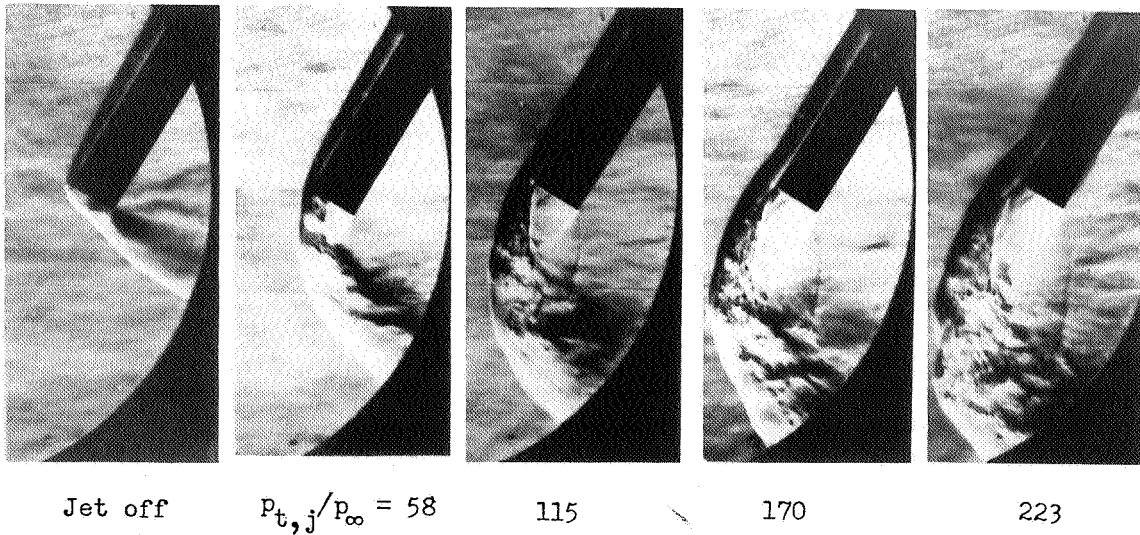
(b) $\alpha = 120°$.   L-61-7747

Figure 6.- Schlieren photographs of flow phenomena near base of model 3.
$R = 0.15 \times 10^6$.
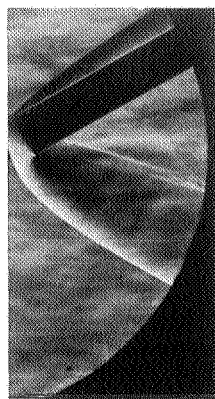
L-1604
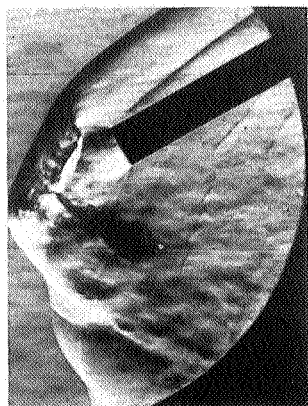
Jet off

$p_{t,j}/p_\infty = 59$

$p_{t,j}/p_\infty = 117$
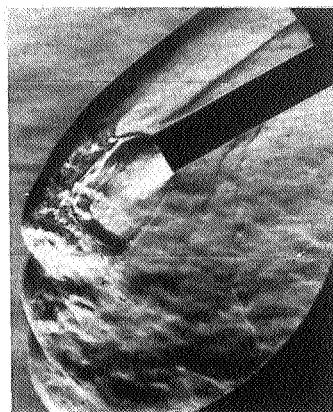
173
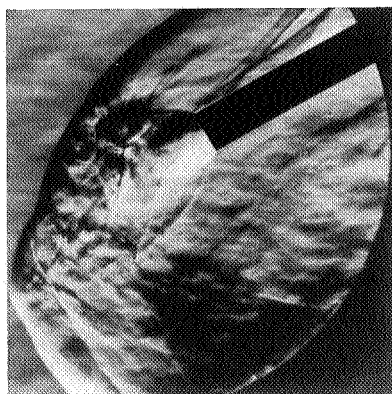
$p_{t,j}/p_\infty = 227$
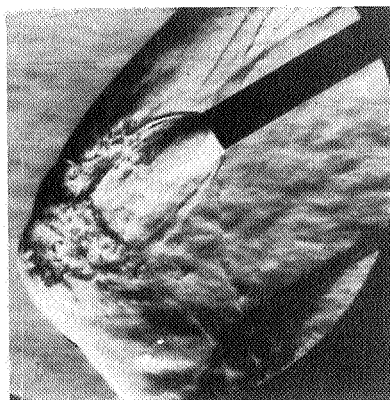
255

(c) $\alpha = 150°$.   L-61-7748

Figure 6.- Continued.

28
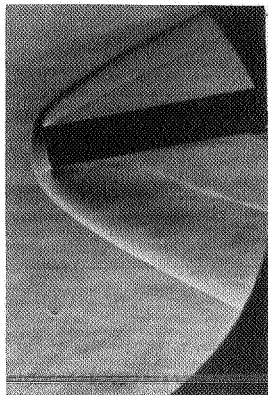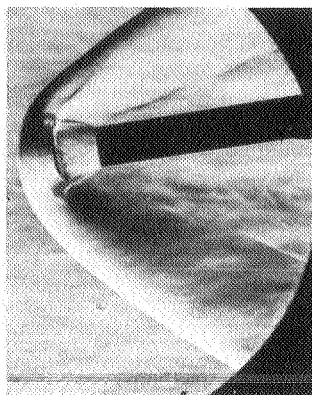
Jet-off

$p_{t,j}/p_\infty = 59$
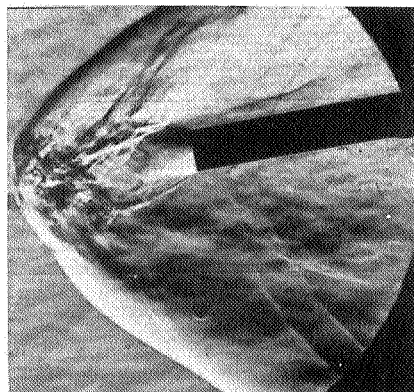
$p_{t,j}/p_\infty = 95$
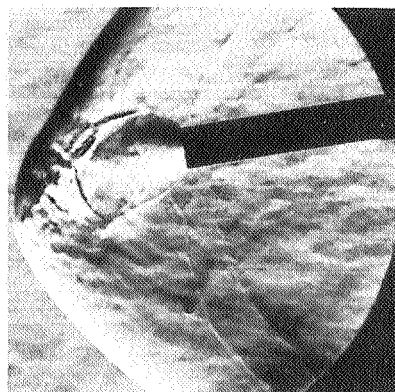
174
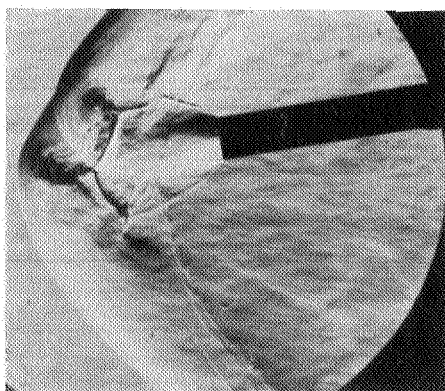
$p_{t,j}/p_\infty = 227$
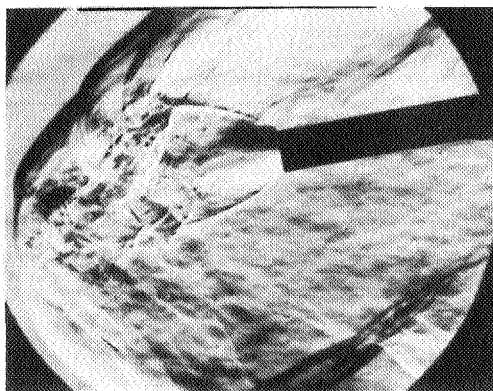
256

(d) $\alpha = 170^\circ$.   L-61-7749

Figure 6.- Continued.

L-1604
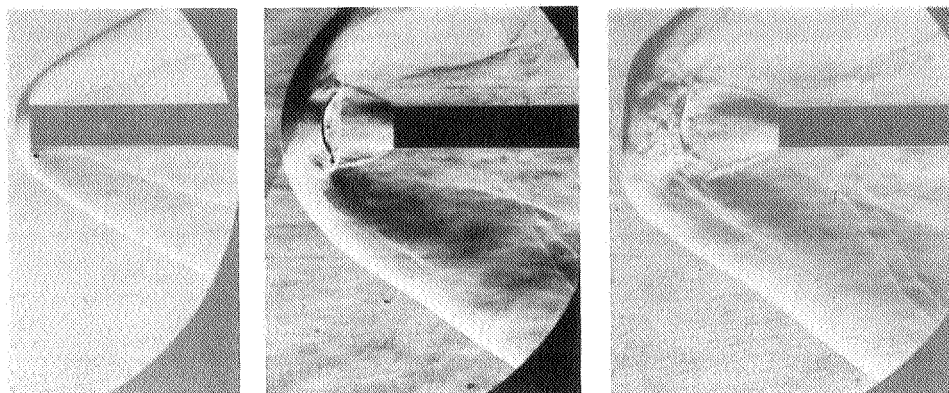
Jet off $p_{t,j}/p_\infty = 89$ 116
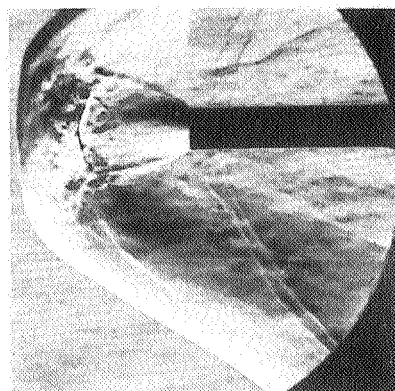
$p_{t,j}/p_\infty = 143$ 172
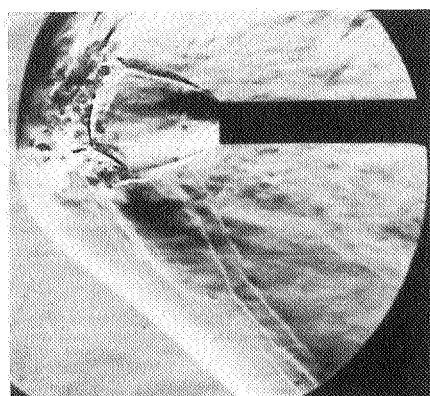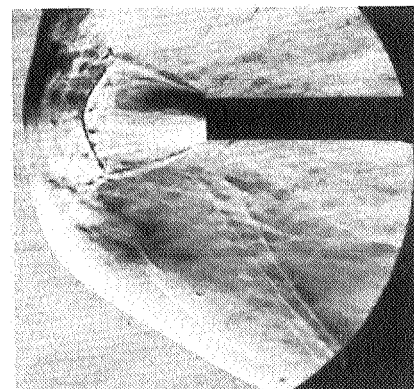
$p_{t,j}/p_\infty = 200$ 228

(e) $\alpha = 180^\circ$.   L-61-7750

Figure 6.- Concluded.

(a) $\phi = 90°$.
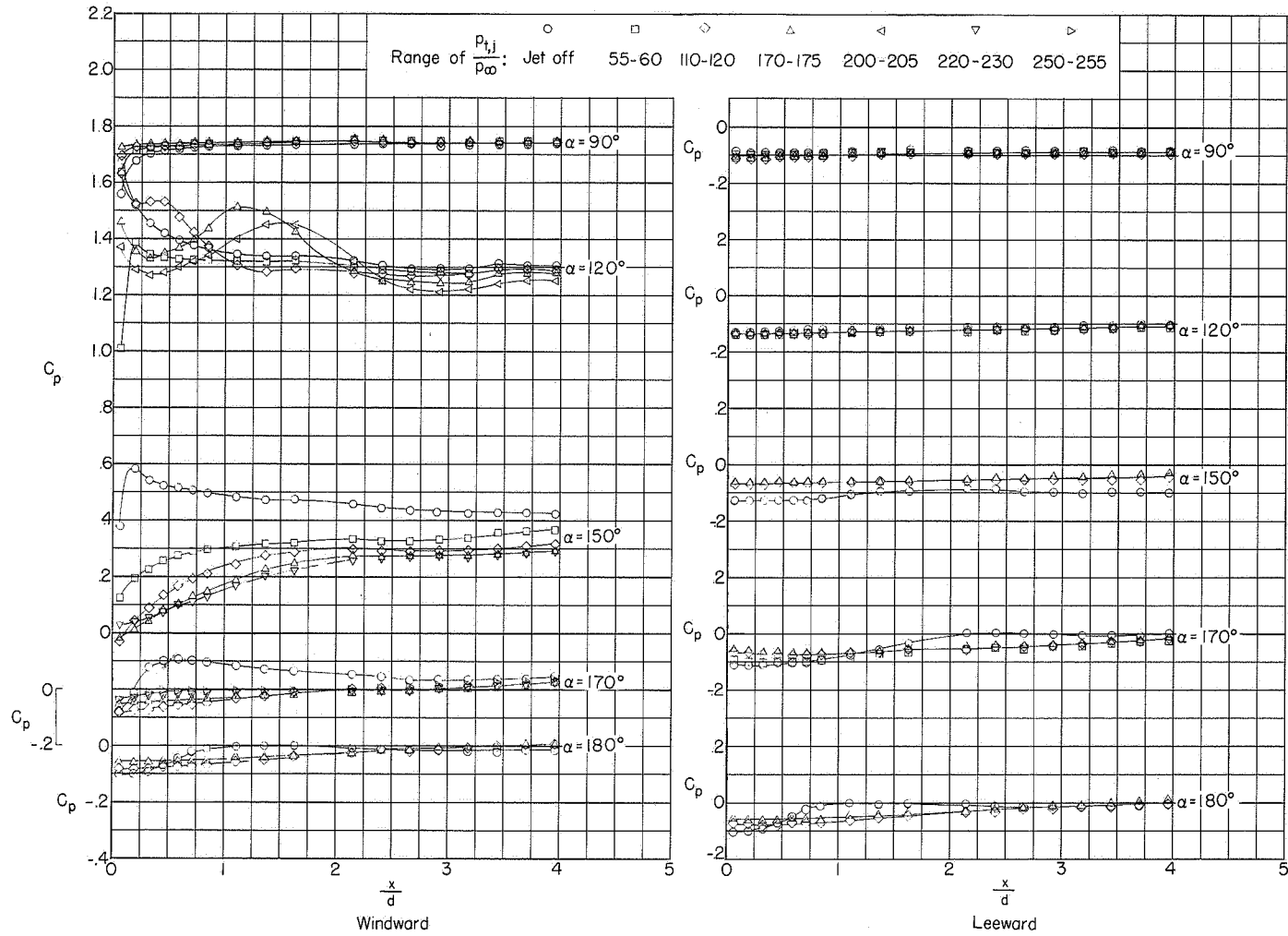
Figure 7.- Pressure distributions on model 1.   R = 0.15 × 10^{6}.
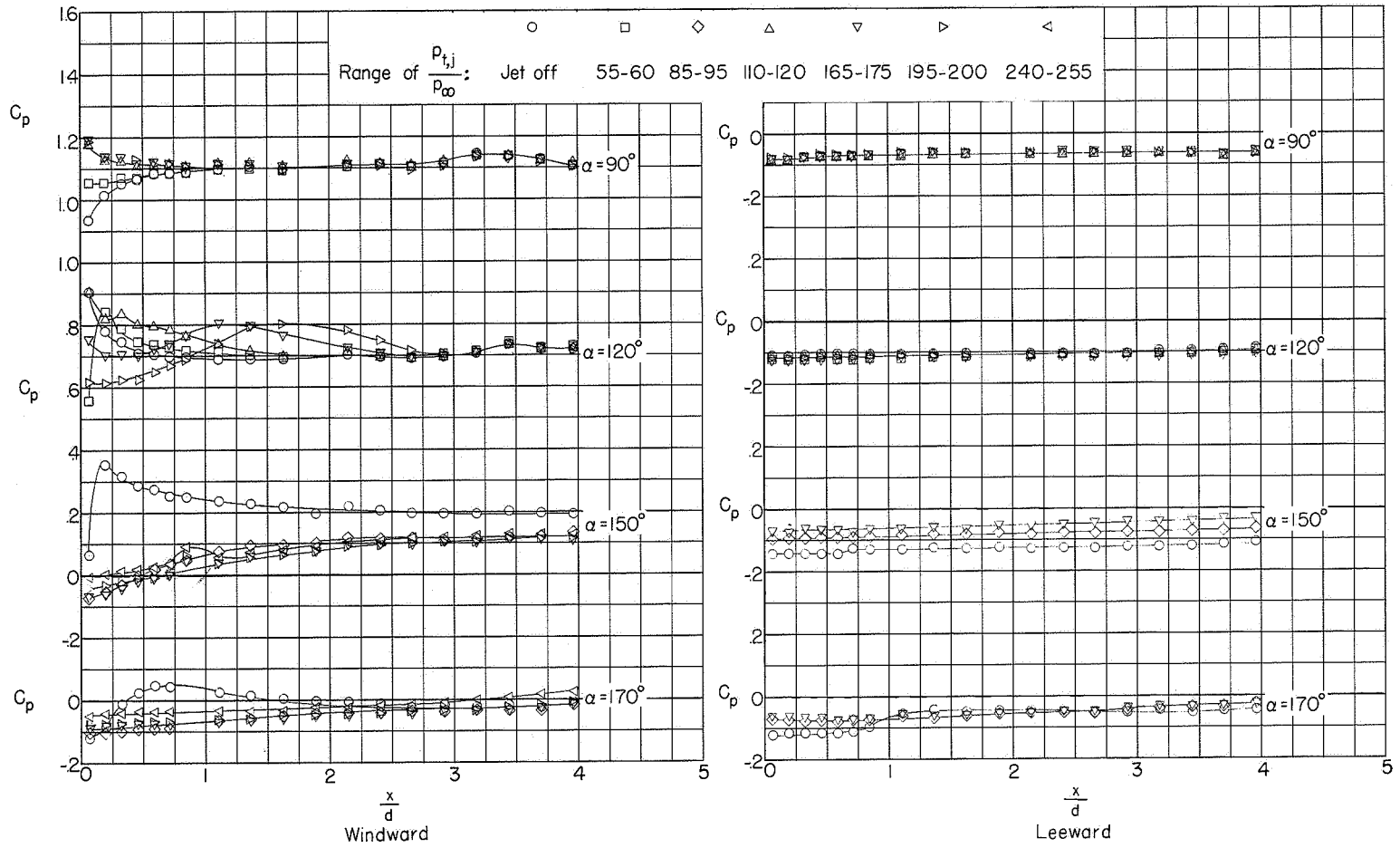
(b) $\phi = 45°$.

Figure 7.- Continued.
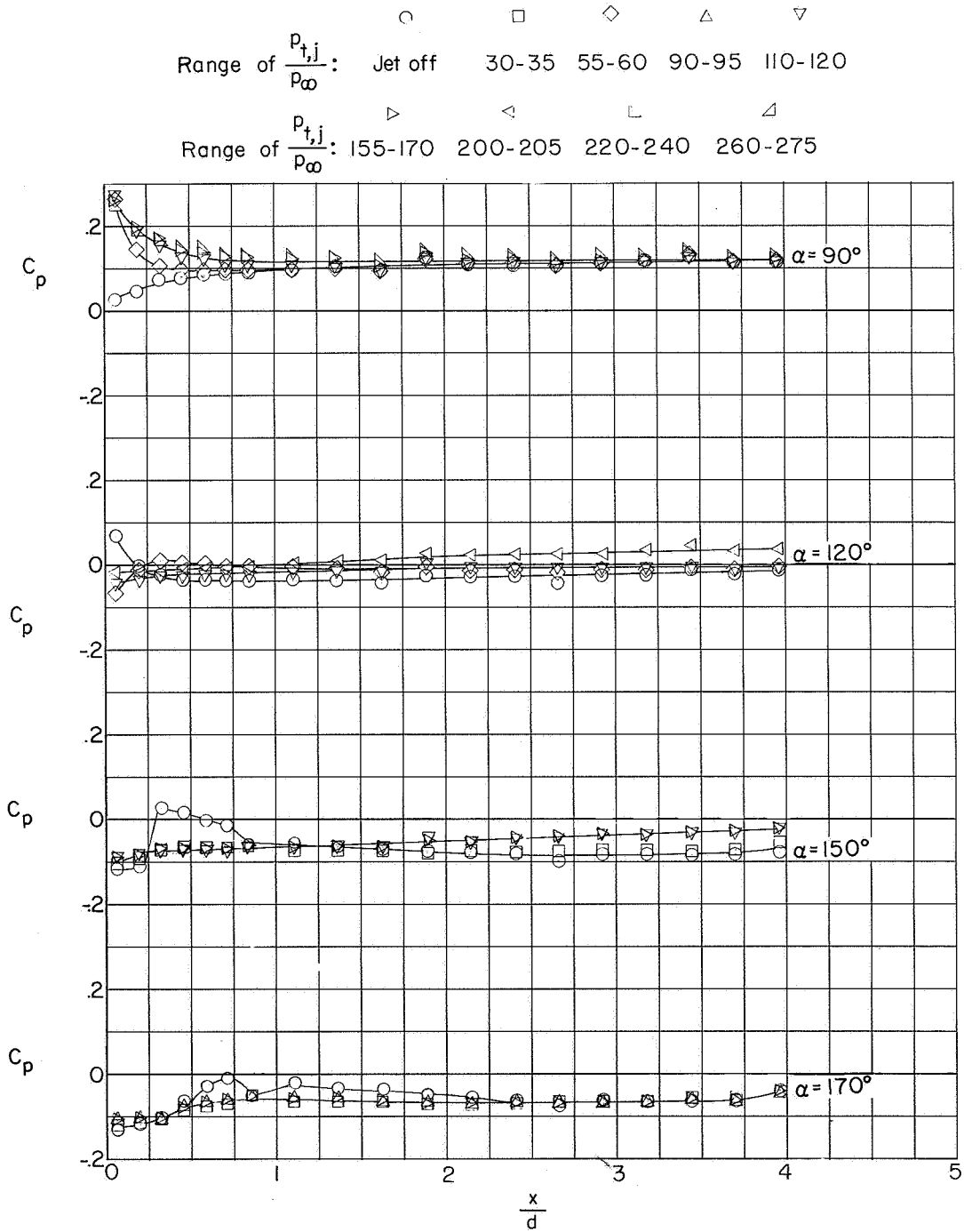
(c) $\phi = 0°$.

Figure 7.- Concluded.
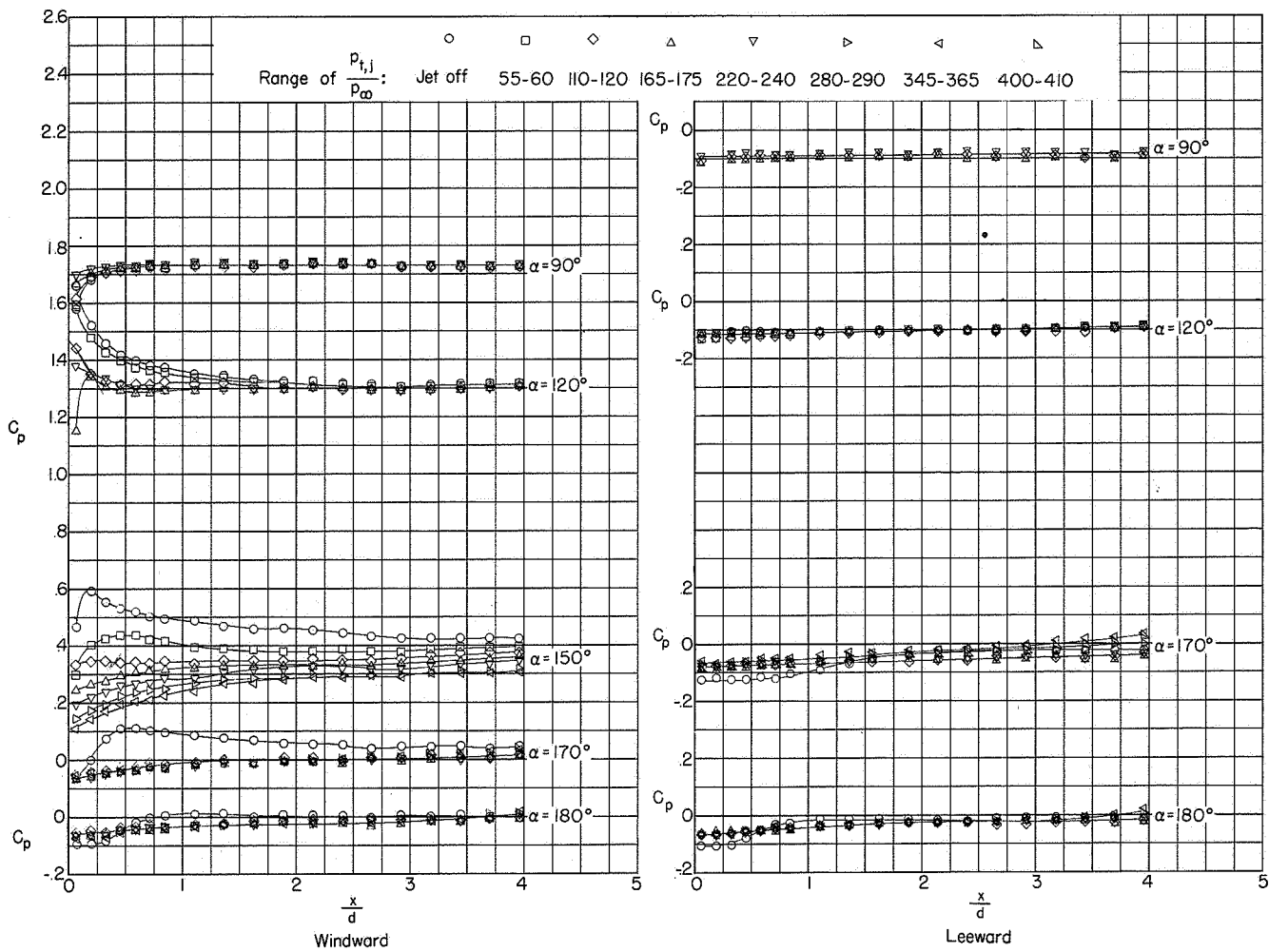
Figure 8.- Pressure distributions on model 2. R = 0.15 × 10⁶.
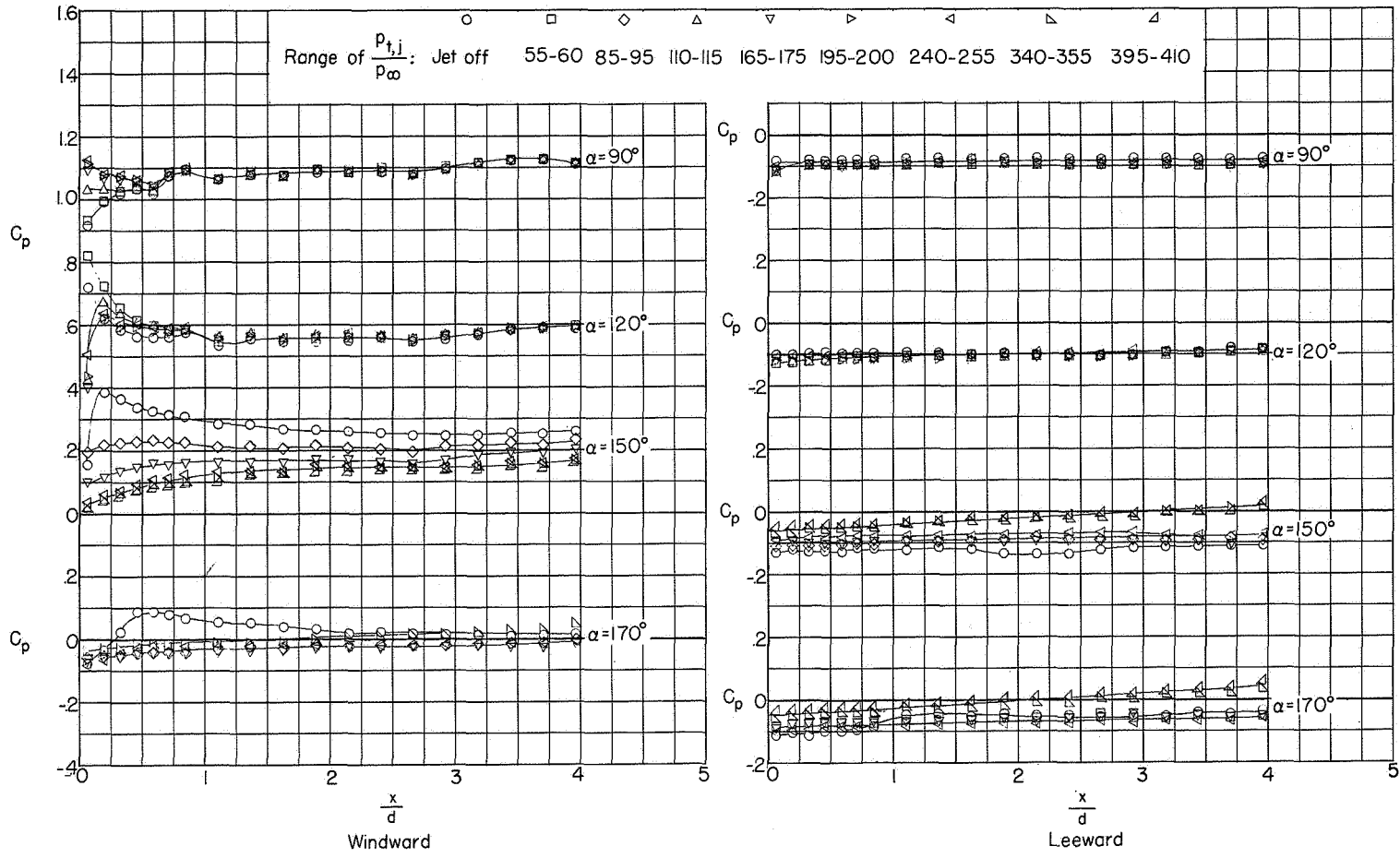
(a) $\phi = 90°$.

(b) $\phi = 45°$.

Figure 8.- Continued.

L-1004
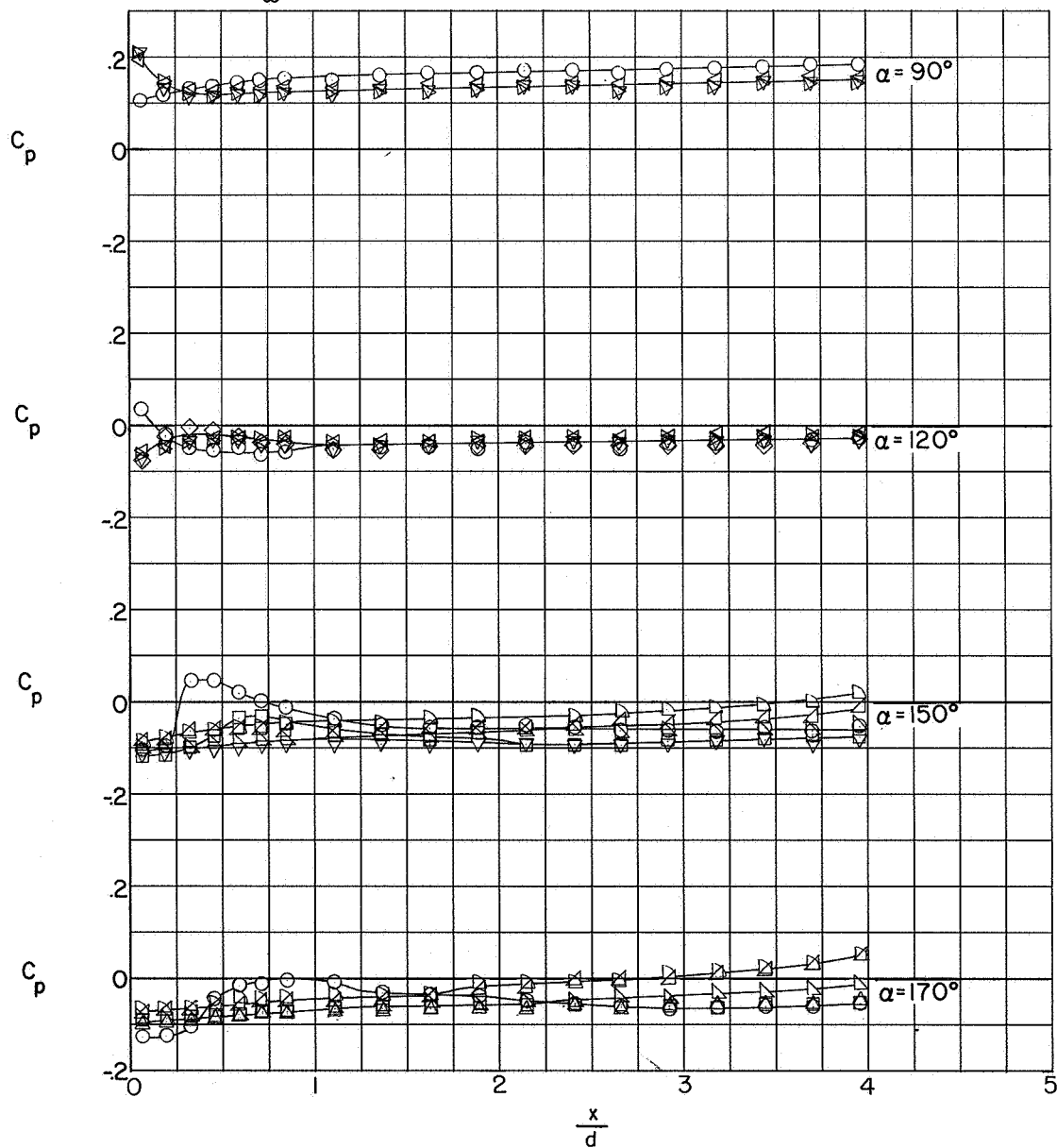
(c) $\phi = 0°$.
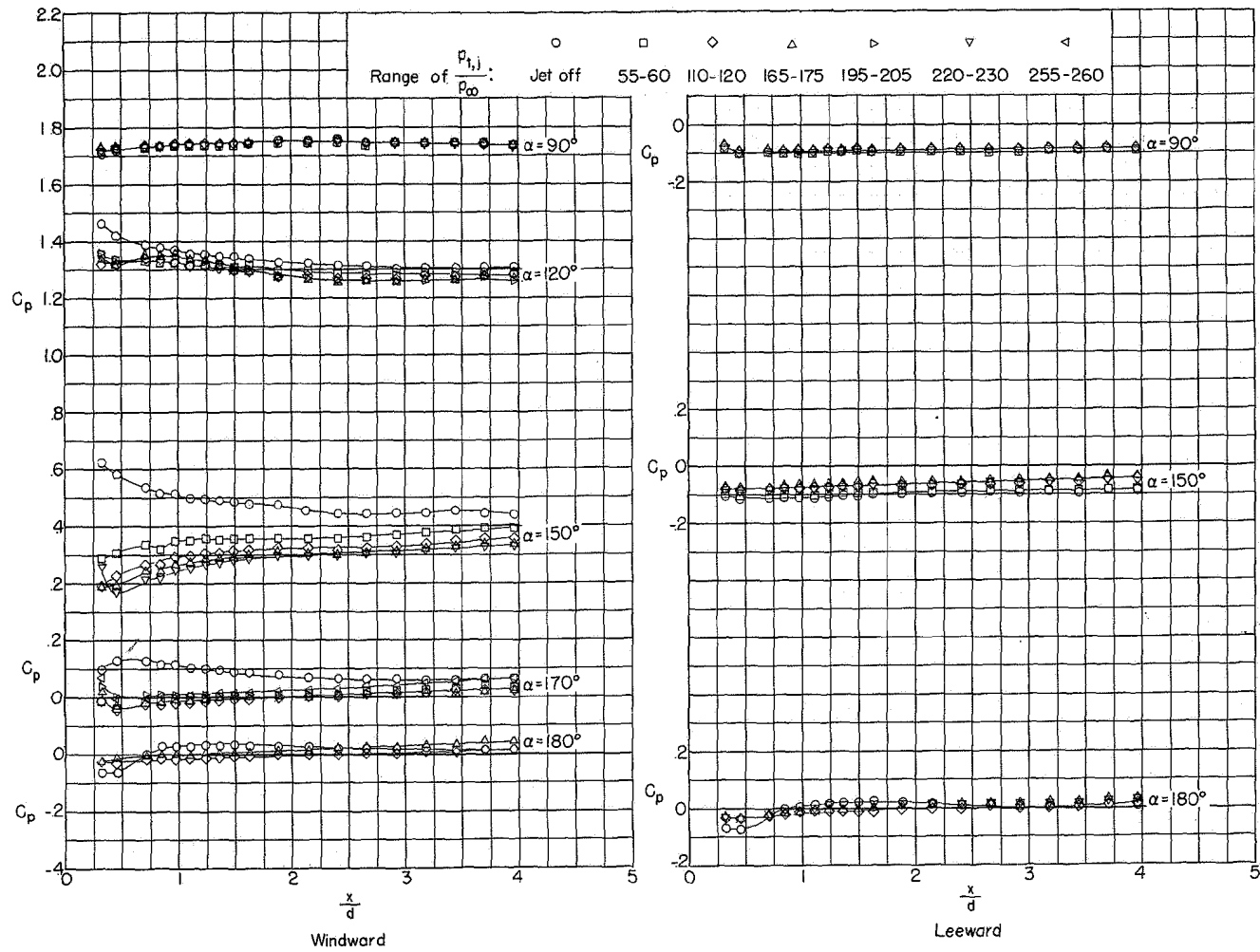
Figure 8.- Concluded.

(a) $\phi = 90°$.

Figure 9.- Pressure distributions on model 3.   R = 0.15 × 10^6.
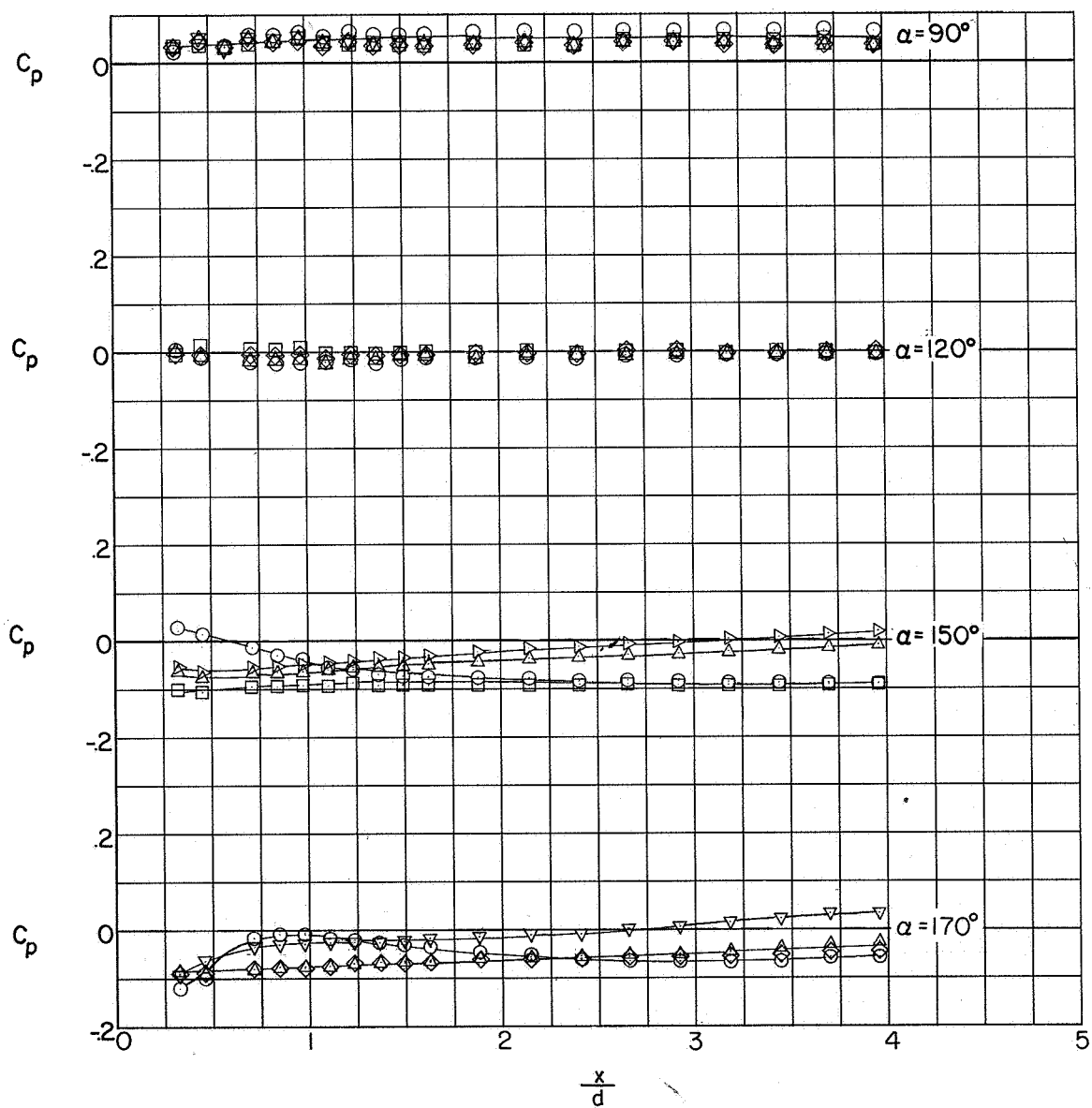
(b) $\phi = 0°$.

Figure 9.- Concluded.
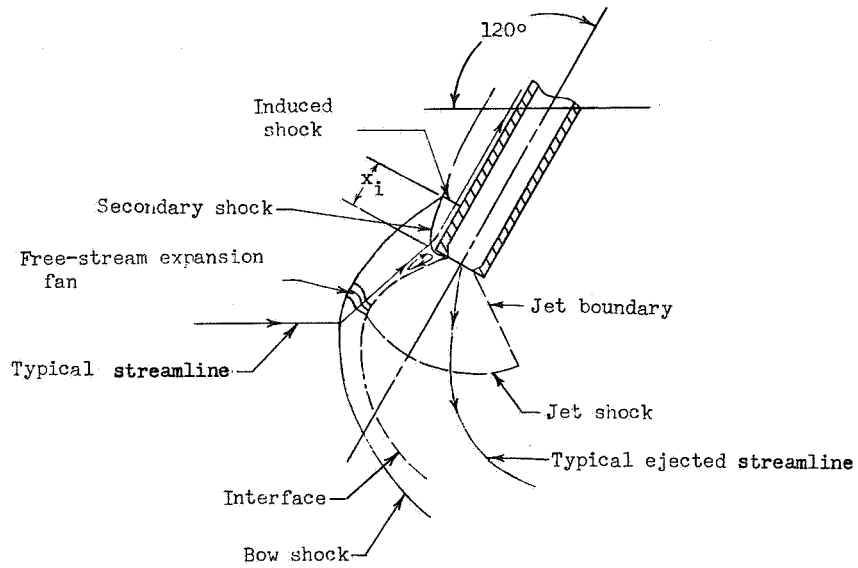
(a) Sketch showing flow field.
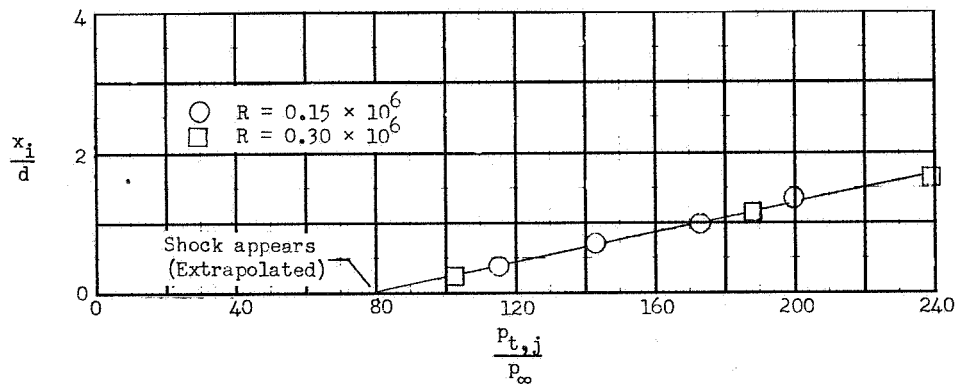
(b) Variation of induced-shock location with jet pressure ratio.

Figure 10.- Sketch of flow field around model 1 showing induced shock and variation of induced-shock location with jet pressure ratio. $\alpha = 120^{\circ}$.
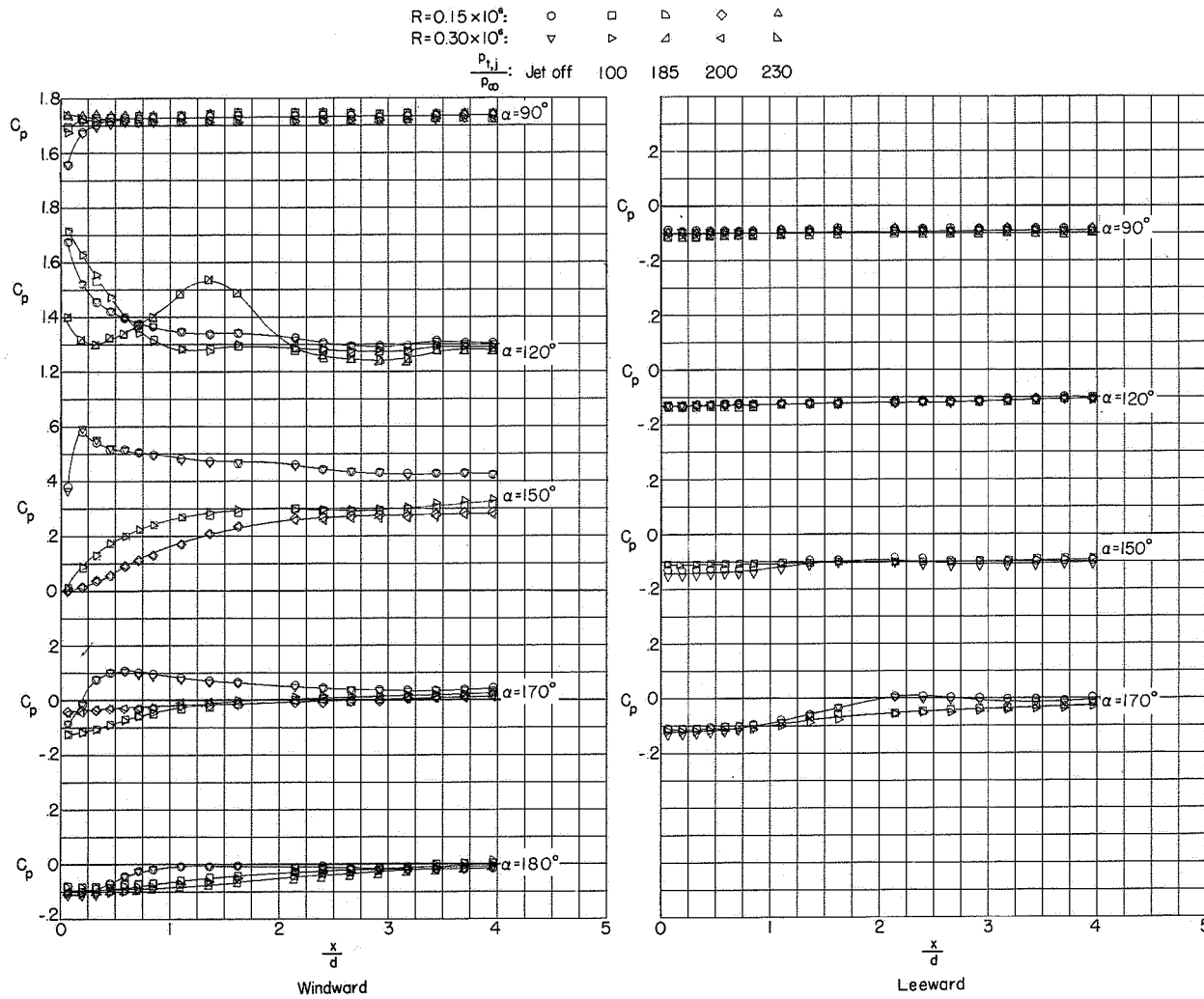
Figure 11.- Effects of Reynolds number on pressure distributions on model 1. $\phi = 90°$.
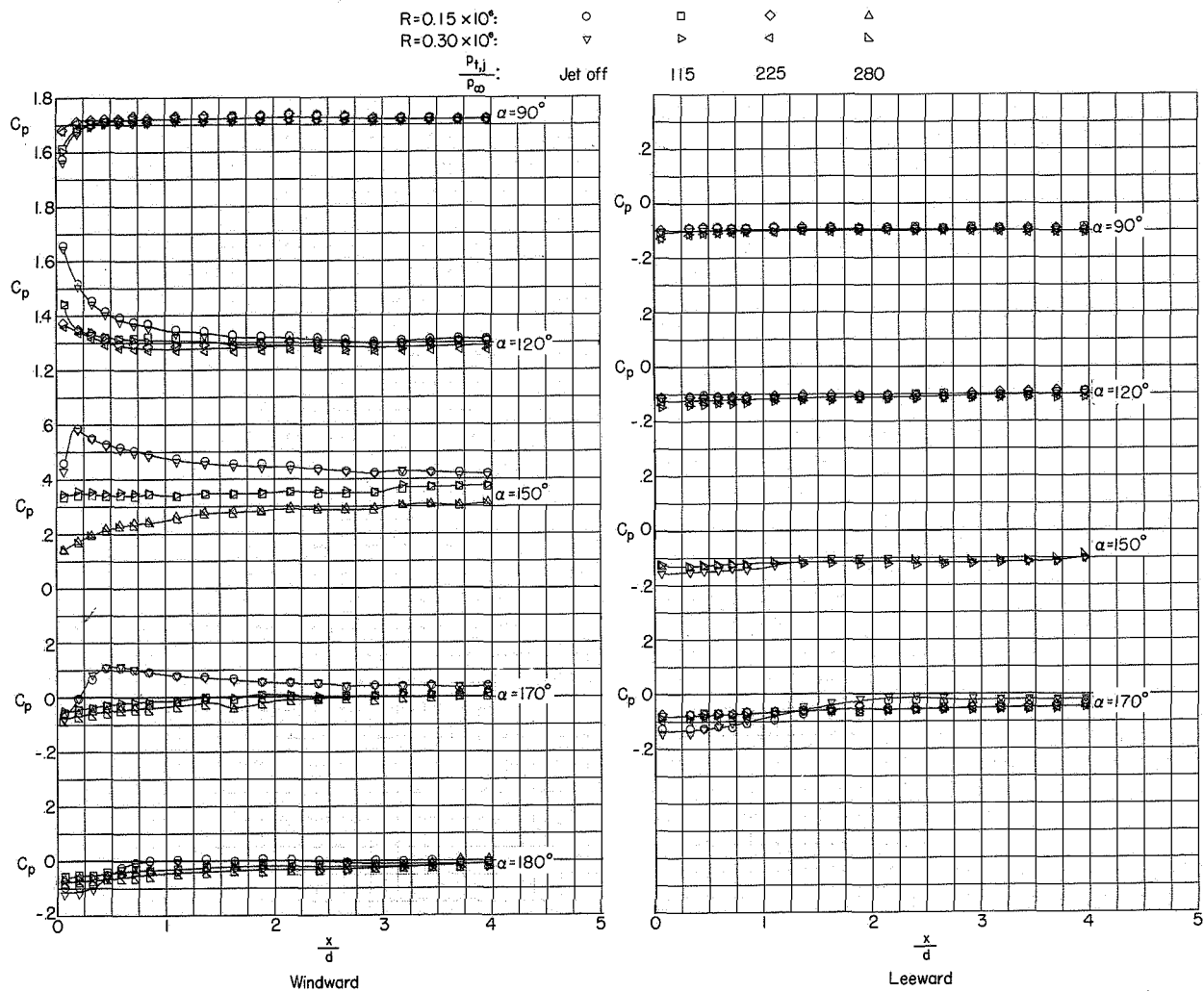
Figure 12.- Effects of Reynolds number on pressure distributions on model 2. $\phi = 90°$.
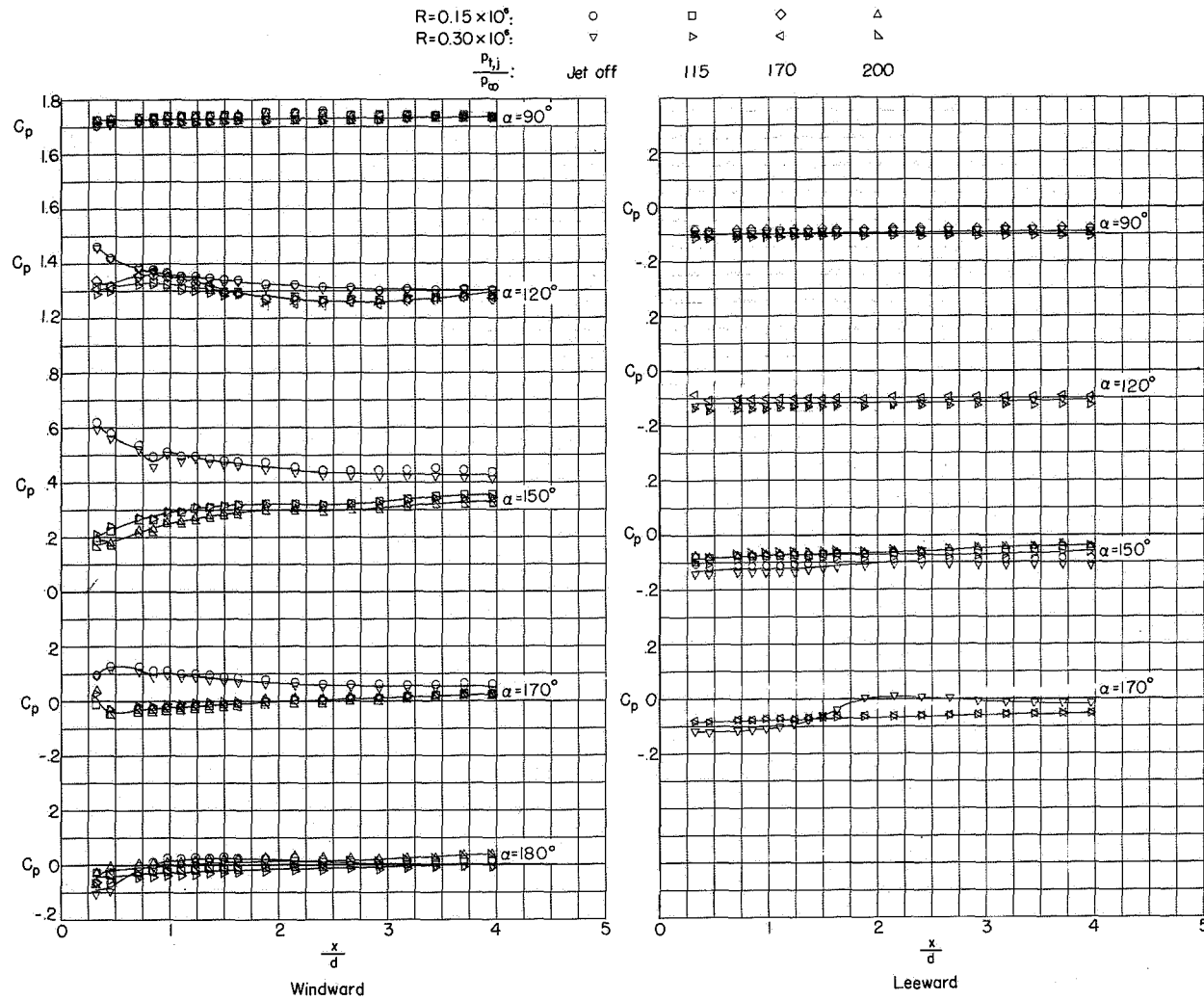
Figure 13.- Effects of Reynolds number on pressure distributions on model 3. $\phi = 90°$.
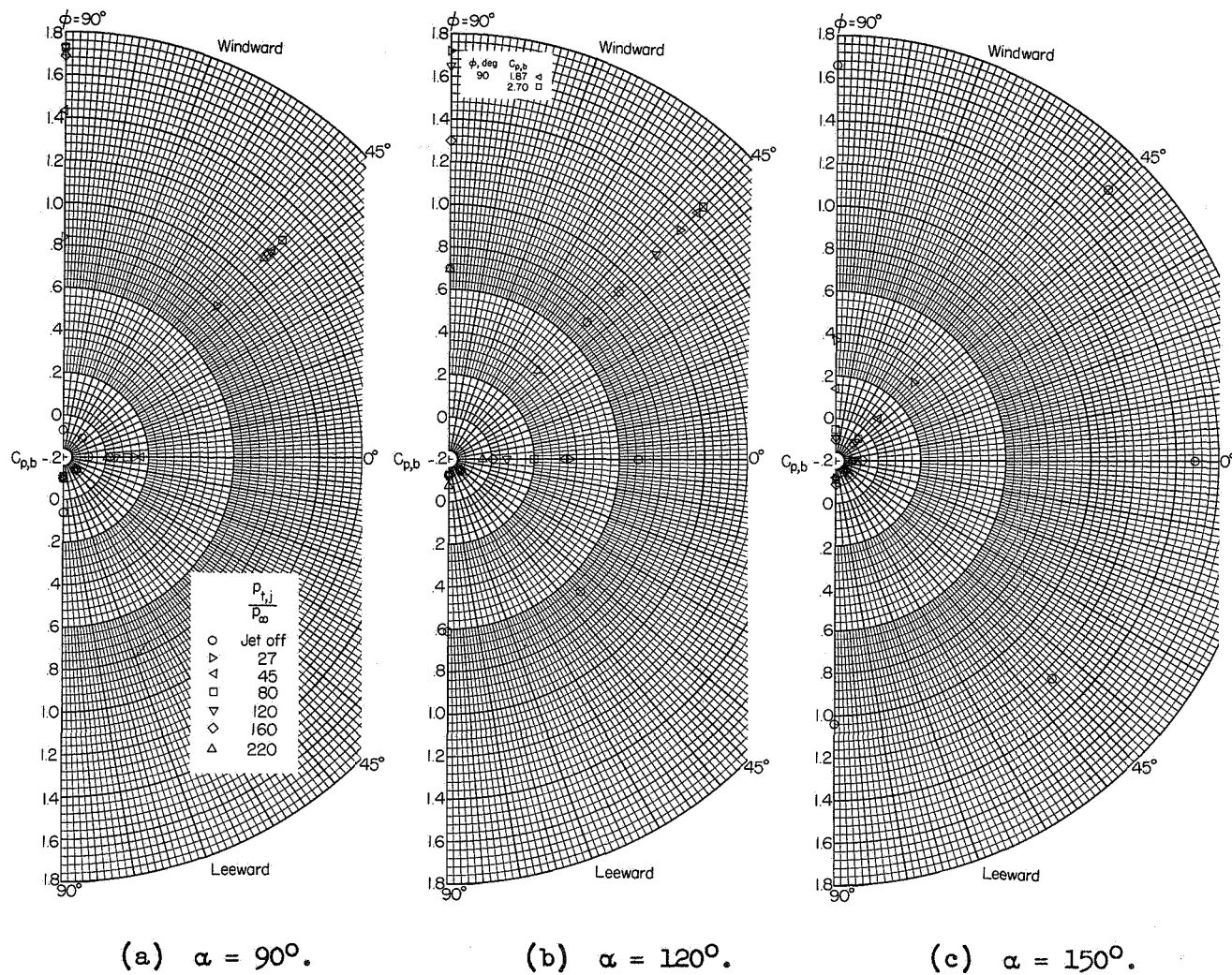
(a) $\alpha = 90°$.   (b) $\alpha = 120°$.   (c) $\alpha = 150°$.

Figure 14.- Effects of jet pressure ratio on the base pressures of model 1 for $R = 0.30 \times 10^6$. $r_0/r_b = 0.582$.
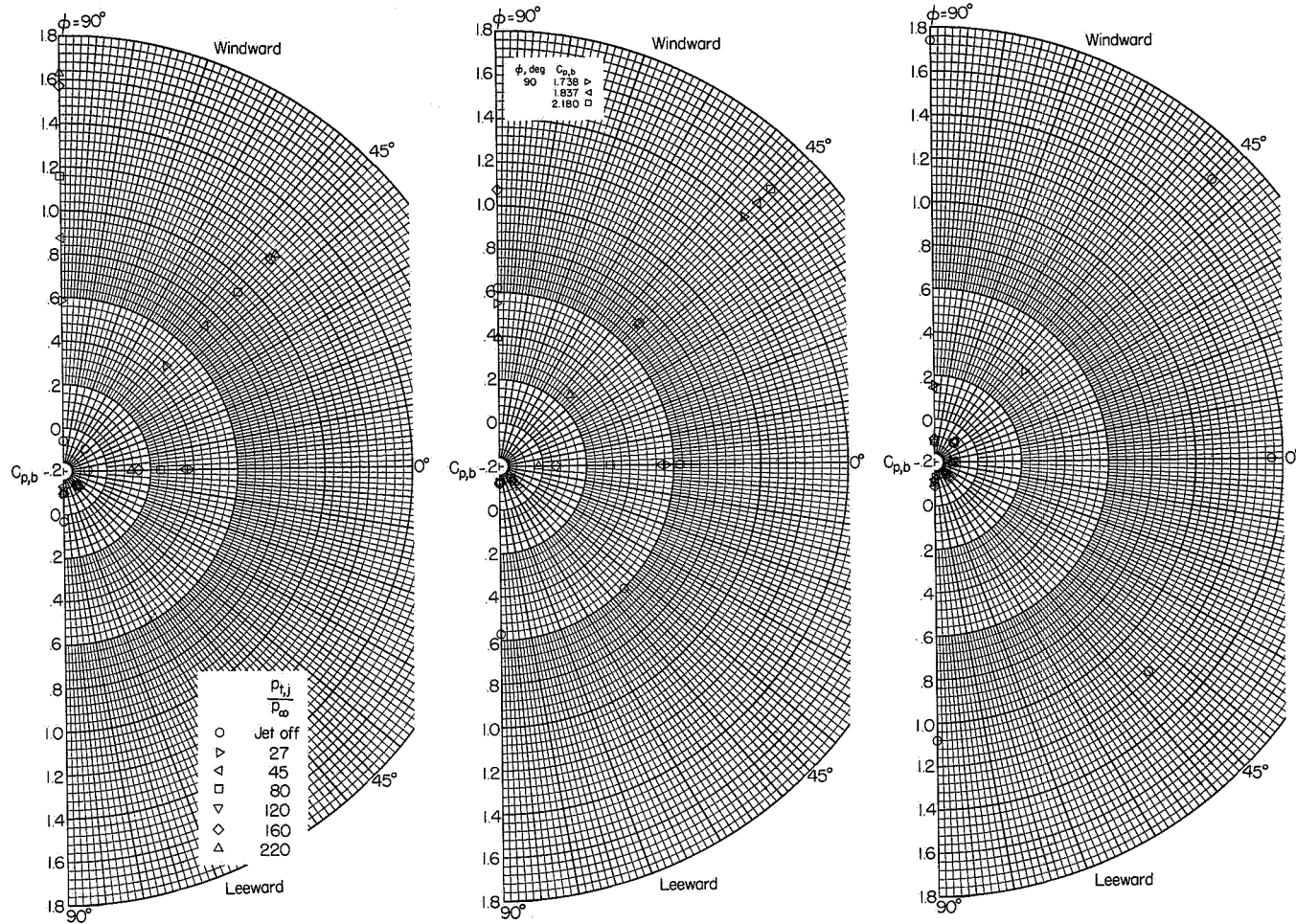
L-1604
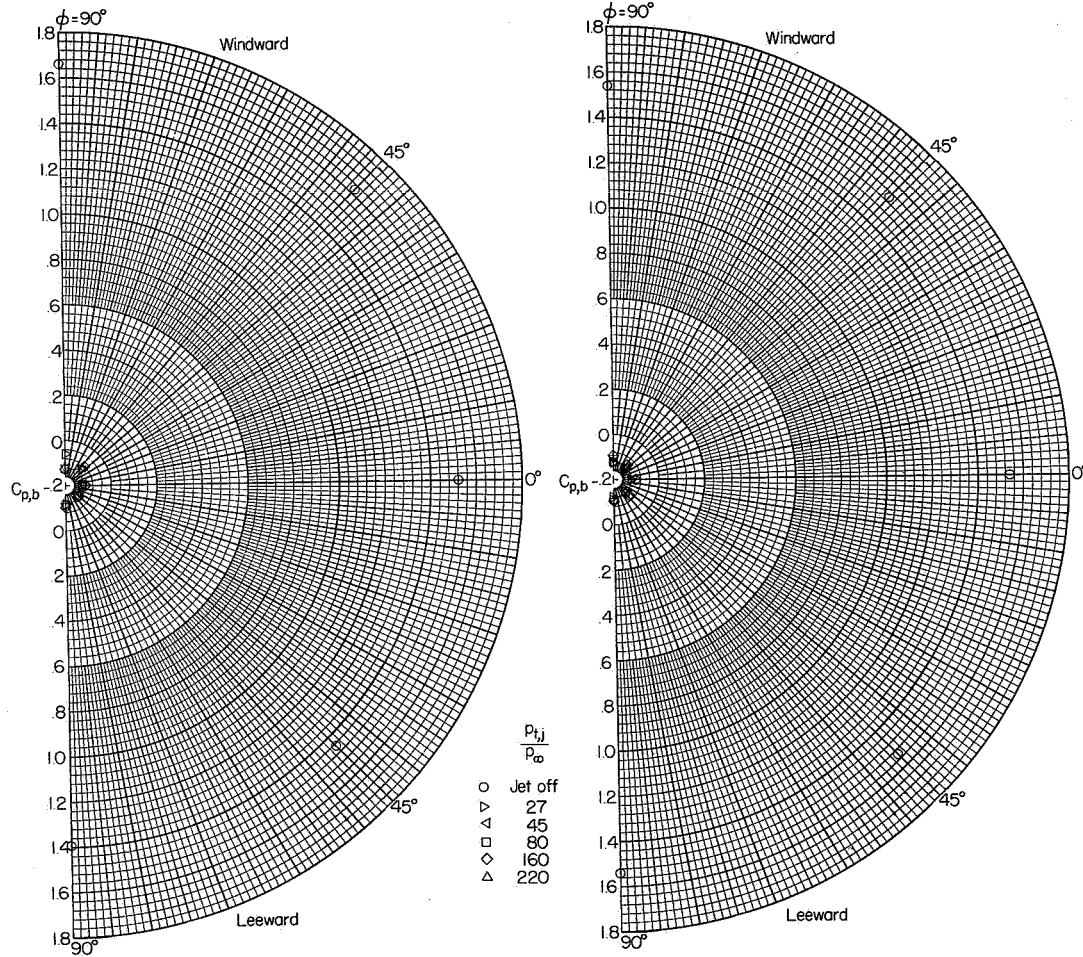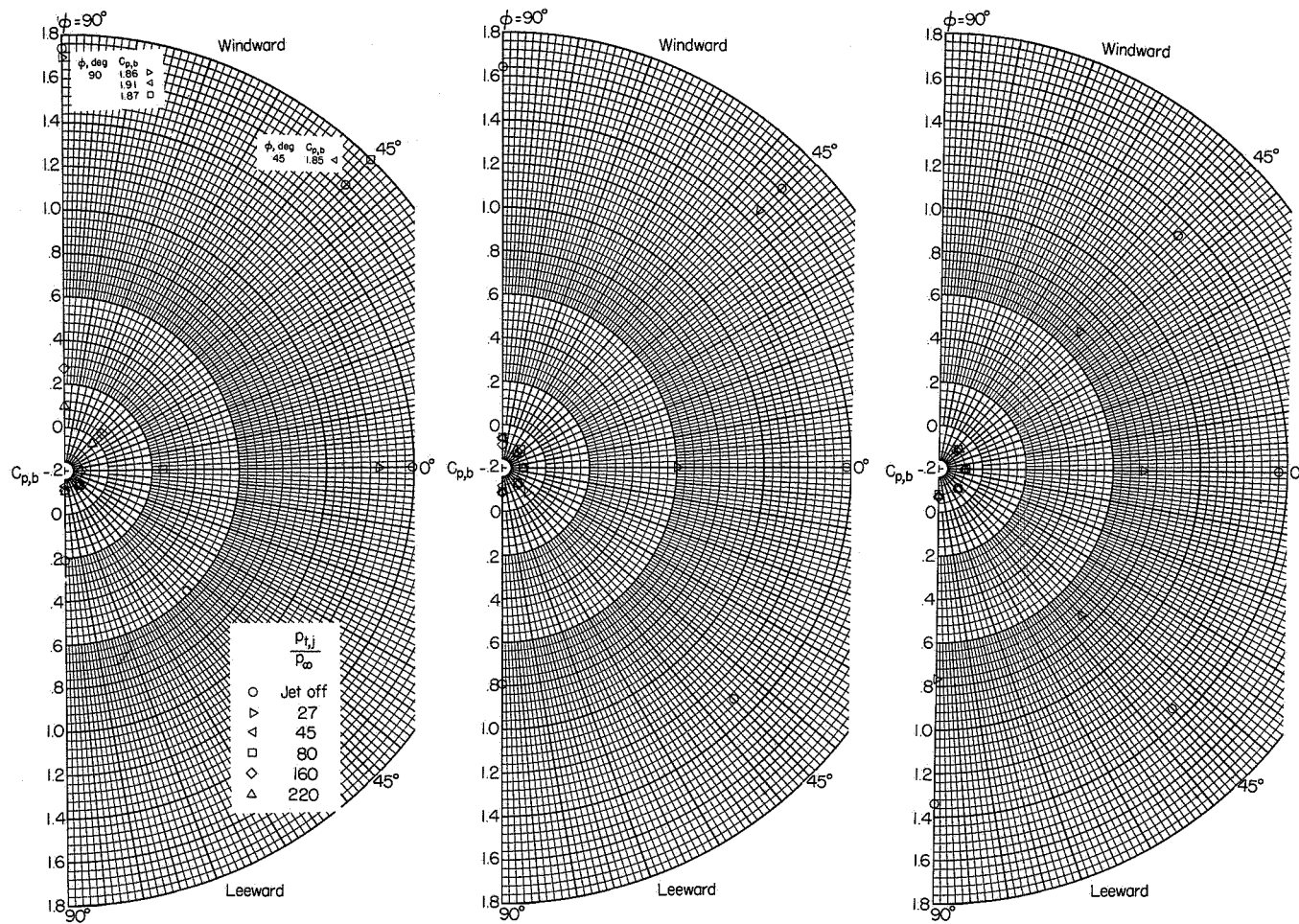

(d) α = 170°.
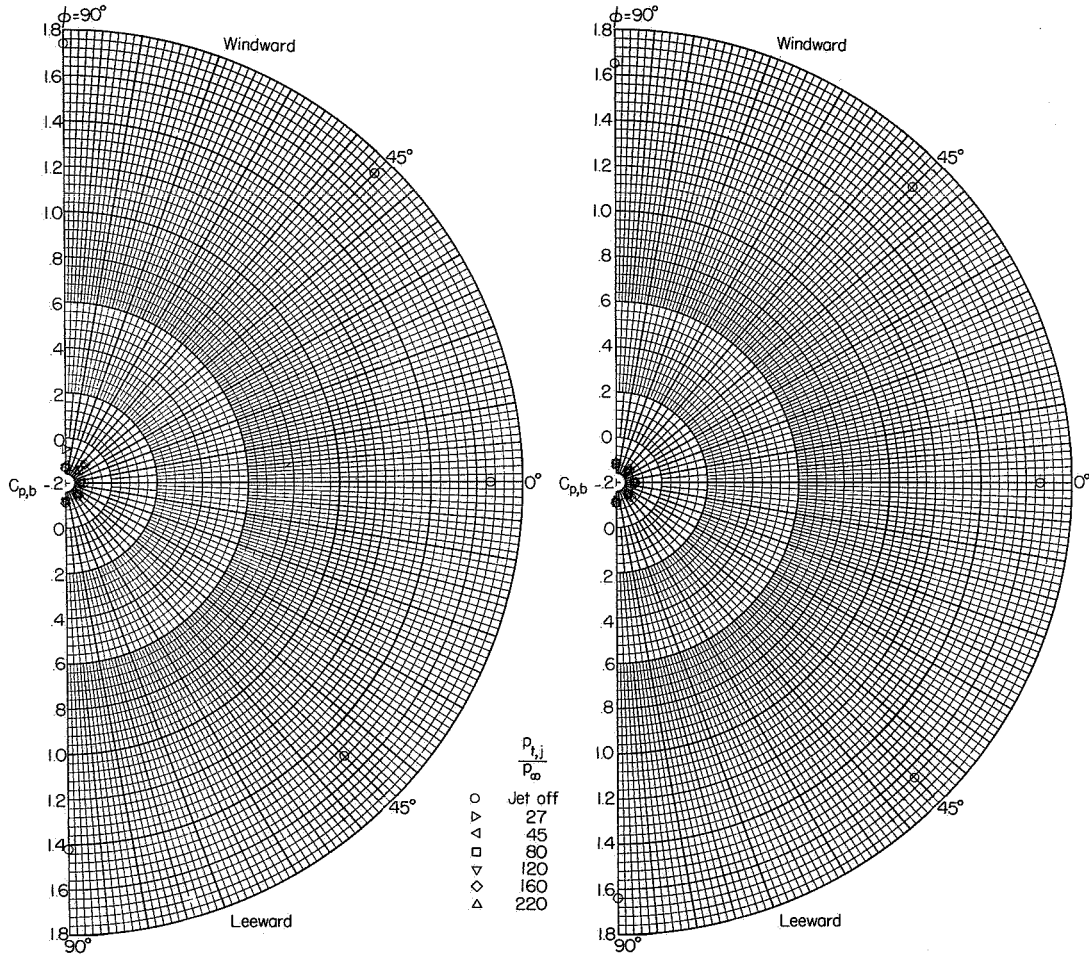
(e) α = 180°.

Figure 14.- Concluded.

(a) $\alpha = 90°$.   (b) $\alpha = 120°$.   (c) $\alpha = 150°$.

Figure 15.- Effects of jet pressure ratio on the base pressures of model 1 for $R = 0.30 \times 10^6$. $r_o/r_b = 0.848$.

L-1604

(d)   α = 170°.

(e)   α = 180°.

Figure 15.- Concluded.

(a) α = 150°.   (b) α = 170°.   (c) α = 180°.

Figure 16.- Effects of jet pressure ratio on the base pressures of model 2 for $R = 0.30 \times 10^6$.
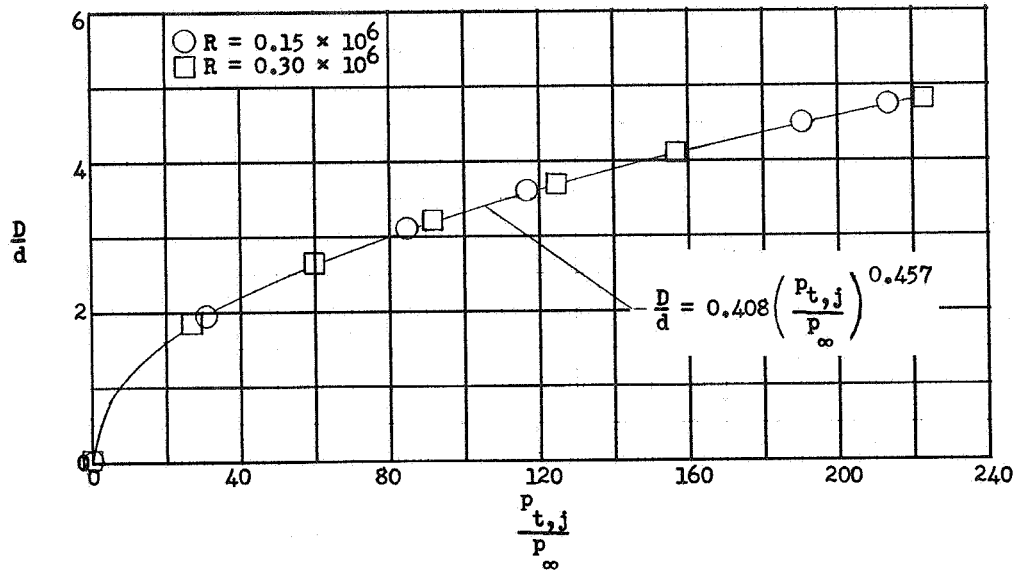$r_o/r_b = 0.880$.

Figure 17.- Variation of interface detachment distance parameter D/d
with jet pressure ratio for model 1 at $\alpha = 180^\circ$.
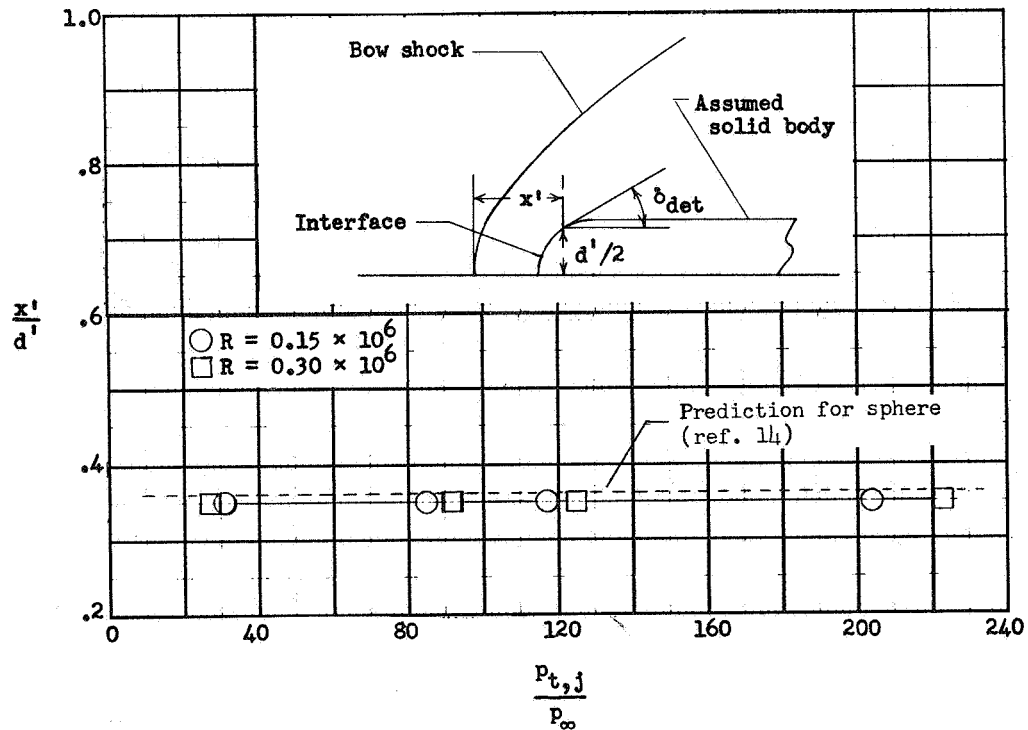

Figure 18.- Experimental and predicted bow-shock detachment distance.
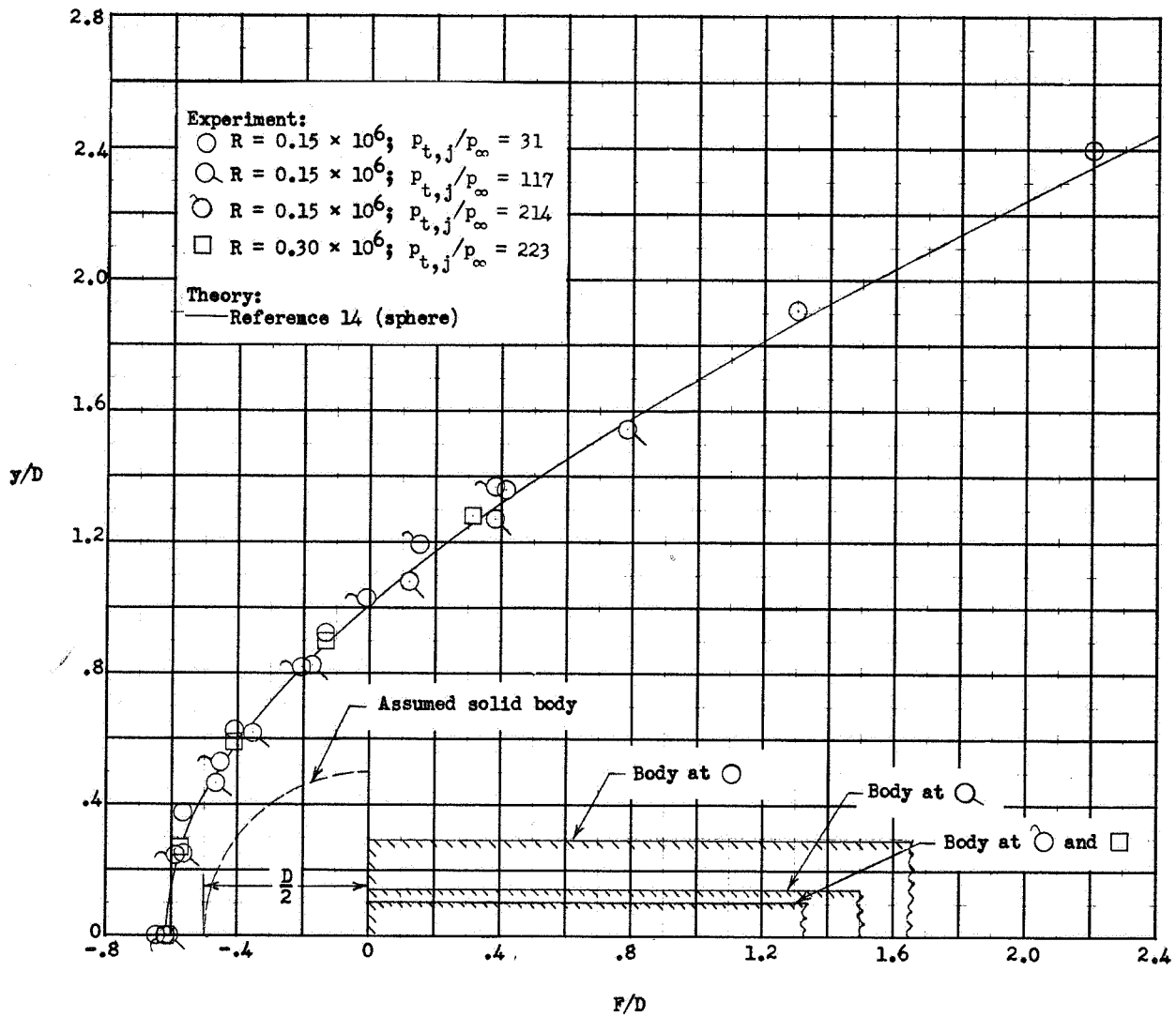Model 1; $\alpha = 180^\circ$.

Figure 19.- Experimental and predicted bow-shock shape and location. Model 1; $\alpha = 180^\circ$.
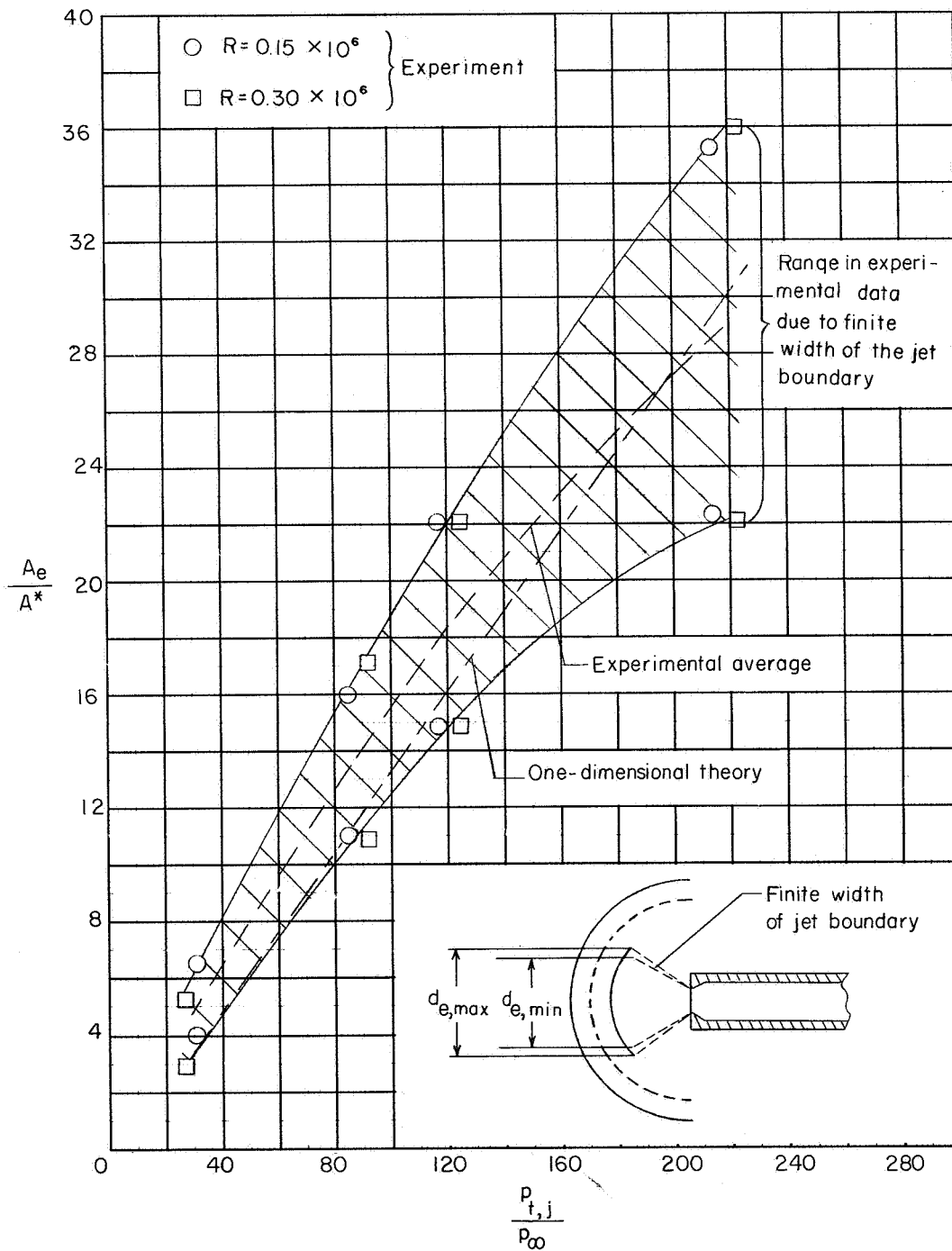
Figure 20.- Comparison of variation of experimental and theoretical expansion of jet flow with jet pressure ratio. (Theory is a combination of one-dimensional channel and normal-shock relations.)